

Weathering without realizing inorganic CO₂ removal revealed through base cation monitoring.

Arthur Vienne¹, Patrick Frings², Jet Rijnders¹, Lucilla Boito¹, Jens Hartmann³, Harun Niron¹, Reinaldy P. Poetra³, Miguel Portillo Estrada¹, Tom Reershemius⁶, Laura Steinwider¹, Tim Jesper Suhrhoff^{4,5}, Sara Vicca¹

¹Biobased Sustainability Engineering (SUSTAIN), Department of Bioscience Engineering, University of Antwerp, Antwerp, Belgium

²GFZ German Research Centre for Geosciences, Section Earth Surface Geochemistry, Telegrafenberg, 14473 Potsdam, Germany

³Institute for Geology, Centre for Earth System Research and Sustainability (CEN), Universität Hamburg, Bundesstraße 55, 20146 Hamburg, Germany

⁴Yale Center for Natural Carbon Capture, Yale University, New Haven, CT 06511, USA

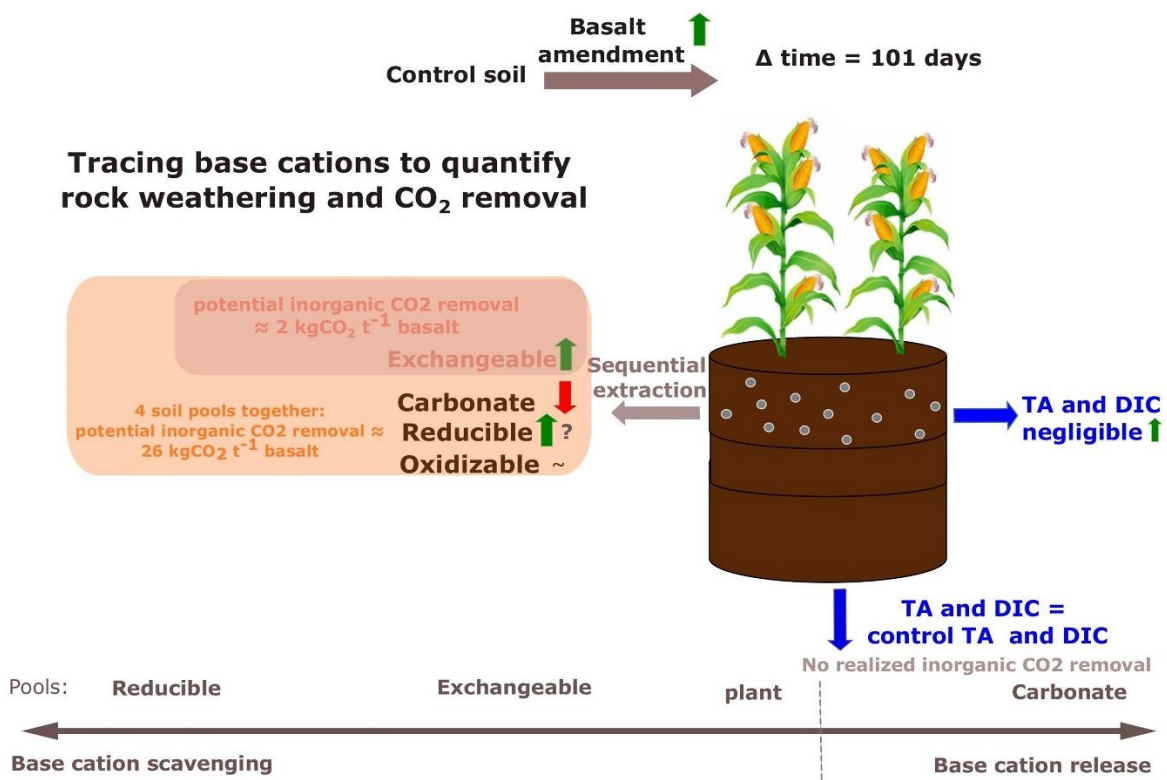
⁵Department of Earth and Planetary Sciences, Yale University, New Haven, CT 06511, USA

⁶School of Natural and Environmental Sciences, Newcastle University, Newcastle upon Tyne, UK

Correspondence to: arthur.vienne@uantwerpen.be; sara.vicca@uantwerpen.be

Keywords: CDR, Enhanced weathering, Monitoring reporting and verification (MRV), sequential extractions, weathering, basalt, time lags for CO₂ removal, secondary minerals

Graphical abstract



Abstract

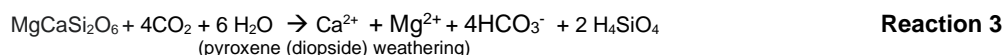
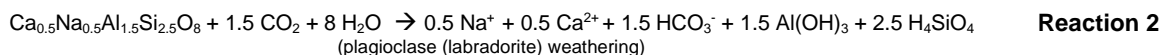
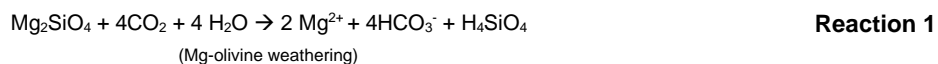
Enhanced Weathering using basalt rock dust is a scalable carbon dioxide removal (CDR) technique, but quantifying rock weathering and CDR rates poses a critical challenge. Here, we investigated realized inorganic CO₂ removal (defined as the sum of the change in dissolved inorganic C leaching and in neoformed solid inorganic C) and weathering rates by treating mesocosms planted with maize with basalt (0, 10, 30, 50, 75, 100, 150 and 200 t ha⁻¹) and monitoring them for 101 days. We observed no significant realized inorganic CO₂ removal, as leaching of dissolved inorganic carbon did not increase, and soil carbonate content declined over time.

30 To gain insights into the weathering processes, we traced the fate of base cations in the soil and plants. This
 31 analysis showed that most base cations were retained in the topsoil reducible soil pool, typically associated with
 32 iron (hydr)oxides, while increases in the exchangeable pool were about a factor 10 smaller. Soil base cation
 33 scavenging exceeded plant scavenging by approximately two orders of magnitude. From the base cations in all
 34 pools (soil, soil water and plants), we quantified log weathering rates of $-11 \text{ mol total alkalinity m}^{-2} \text{ basalt s}^{-1}$. The
 35 potential inorganic CO_2 removal, defined as the maximum inorganic CO_2 removal achievable if all weathered base
 36 cations, adsorbed by soil pools in this experiment, would leach out of the soil and be fully balanced by carbonate
 37 anions, was estimated at $26 \text{ kg CO}_2 \text{ t}^{-1} \text{ basalt}$.

38 In conclusion, despite clear weathering of basalt rock, we found no inorganic CO_2 removal within the timescale of
 39 this experiment. The observed increase of aluminum in association with the reducible soil fraction indicate the
 40 formation of secondary minerals. These, along with enhanced base cation exchange, may contribute to long-term
 41 soil fertility and promote the stabilization of soil organic matter.

42 1. Introduction

43 To meet the "well below 2°C warming" target established by the United Nations' Paris Agreement, Carbon Dioxide
 44 Removal (CDR) must complement conventional climate change mitigation efforts (Minx et al., 2018). One CDR
 45 technology under consideration is enhanced weathering (EW). EW relies on accelerating natural weathering
 46 reactions of silicate minerals with water (H_2O) and carbon dioxide (CO_2) (as in **Reactions 1 to 3**), which increases
 47 the concentration of base cations and dissolved inorganic C (DIC) in water, delivering inorganic CO_2 removal. In
 48 this study, [rather than aiming to quantify a full greenhouse gas budget](#), we focus on DIC export from soils to the
 49 ocean. [This pathway is considered the most durable form of carbon sequestration, storing C on timescales](#)
 50 [exceeding those required for climate change mitigation as this pathway is considered the most durable form of](#)
 51 [carbon sequestration \(Phil Renforth & Henderson, 2017\)](#). (Phil Renforth & Henderson, 2017; [Robert A. Berner,](#)
 52 1991), [rather than aiming to quantify a full greenhouse gas budget](#). DIC (the sum of aqueous $[\text{CO}_2]$, $[\text{HCO}_3^-]$ and
 53 $[\text{CO}_3^{2-}]$) can either be measured directly or estimated indirectly from total alkalinity (TA) or electrical conductivity,
 54 which are less expensive to monitor and can be empirically linked with DIC through calibration curves (Amann &
 55 Hartmann, 2022) (see also **Fig. S10**). This calibration is feasible because, according to the explicit conservative
 56 expression for TA in water, $\text{TA} = [\text{HCO}_3^-] + [\text{CO}_3^{2-}] + [\text{OH}^-] - [\text{H}^+]$ ([Bijma et al., 2026; Wolf-Gladrow et al., 2007](#)).
 57 ([Wolf-Gladrow et al., 2007](#)). TA can also be approximated from the sum of base cation charges, minus the sum of
 58 conservative anion charges (e.g. chloride, sulphate, phosphate, nitrate) (Barker, 2013; Wolf-Gladrow et al., 2007).
 59 DIC can also precipitate as soil inorganic carbon (SIC) in the form of solid carbonates, thereby losing half of the
 60 initially captured CO_2 (**Reaction 4**) (Haque et al., 2019). Inorganic CO_2 removal can be defined as the sum of
 61 changes in DIC leaching from a soil system after rock amendment plus the change in solid inorganic C (SIC) within
 62 the soil system after rock amendment. A robust and reliable accounting of Inorganic CO_2 removal must thus include
 63 both monitoring of DIC leaching and SIC changes.



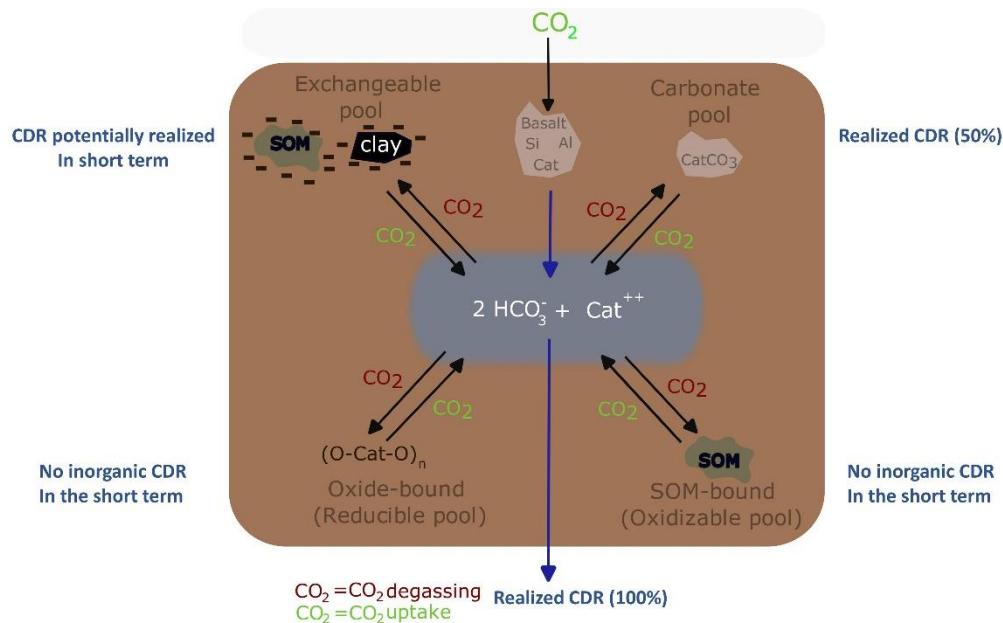
64 EW is an attractive CDR technology for several reasons. First, EW may provide long-lived to permanent CO_2
 65 sequestration: if fixed, DIC is transported via rivers or groundwater to oceans where it may not be released back
 66 into the atmosphere for millennia, the timescale needed for oceanic carbonate precipitation, which would release

67 50% of the DIC input back into the atmosphere (**Reaction 4**) (Renforth & Henderson, 2017). Secondly, rock dust
68 amendment has the potential to improve soil fertility and counters soil acidification (Swoboda et al., 2021; Van
69 Straaten, 2006). Thirdly, unlike some other CDR technologies (such as bio-energy with carbon capture and storage
70 or afforestation), EW avoids competition for land with food production (Fuss et al., 2018; Janssens et al., 2022;
71 Smith et al., 2016). Although several rock types are considered for EW, basalt is typically used in EW field trials
72 and has several advantages. Basalt has relatively high base cation content, particularly of calcium (Ca) and
73 magnesium (Mg), which translates into a high potential for CO₂ removal (Renforth et al., 2019). Additionally, basalt
74 is ~~comprised~~ composed of mafic silicate minerals such as plagioclases, pyroxene, and olivine, known for their
75 relatively high weathering rates (Wr). Furthermore, basalt formations are abundant, widely distributed and close to
76 major economies, making the adoption of EW using basalt scalable. Importantly, basalt is safer for agricultural
77 application compared to ultramafic rocks like dunite due to its lower content of heavy metals such as nickel (Ni)
78 and chromium (Cr) (Beerling et al., 2020).

79 Despite the great potential of terrestrial EW and substantial attention by industry in recent years, monitoring rock
80 weathering and CDR is challenging. Quantification of Inorganic CO₂ removal by EW has often focussed on tracking
81 DIC or alkalinity leaching in porewaters (Holzer et al., 2023; McDermott et al., 2024). However, it is also important
82 to consider DIC in exported soil water (leachates)(Larkin et al., 2022) as changes in DIC during soil water transport
83 are well-established. Numerous studies demonstrated that soil water movement and pH strongly govern DIC
84 dynamics, both in soil research (Öquist et al., 2009; Schindlbacher et al., 2019) and in EW research (Dietzen et al.,
85 2018; Niron et al., 2024; Reynaert et al., 2023; Vienne et al., 2024).

86 Focusing solely on changes in DIC and SIC may however overlook other critical soil processes that impact CDR.
87 Besides the carbonate soil pool, other solid soil pools can also extract base cations from solution (**Figure 1**). These
88 pools (temporarily) trap base cations, preventing DIC leaching and could stabilize soil organic matter (SOM) (Buss
89 et al., 2024). Here, we trace the fate of cations in four different soil pools, to gain better estimates of Wrs and CDR.

90



91

92 **Figure 1:** Schematic representation of aluminosilicate rock weathering and four soil pools that
 93 scavenge base cations (= alkalinity): exchangeable pool, carbonate pool, reducible pool and oxidizable pool.
 94 Because of charge balance, uptake of base cations by these pools releases H⁺ that can convert bicarbonate
 95 (HCO₃⁻) (that was a priori generated from CO₂ through weathering) into CO₂. Cat⁺⁺ = one divalent base cation or
 96 two monovalent base cations. In each corner, in blue, the significance for CDR is indicated for each of the soil pools.
 97 Realized CDR (100%) means that all alkalinity produced by mineral weathering is fully leached from the soil,
 98 achieving the maximum possible inorganic CO₂ removal for that amount of weathering. In contrast, Realized CDR
 99 (50%) accounts for pedogenic carbonate formation (e.g., Reaction 4), where half of the alkalinity released by
 100 weathering is consumed locally, reducing the inorganic CO₂ removal by 50%.

101 Tracing base cations in soils can be done based on the established methodology of Tessier et al. (1979) in which
 102 cations are partitioned into four operationally defined soil pools; The exchangeable pool, the carbonate pool, the
 103 reducible pool and the oxidizable pool. First, in the exchangeable soil pool, cations interact with negatively charged
 104 clay or SOM surfaces. Exchangeable pool cations form relatively weak chemical bounds in a diffuse layer or with
 105 outer-sphere-interactions (Blume et al., 2016). Secondly, the carbonate pool contains carbonates such as calcium
 106 carbonate (CaCO₃) and the C in this pool is reported as SIC. The detection of changes in SIC in basalt amended
 107 soils in short-duration experiments is typically challenging (Kelland et al., 2020; Vienne et al., 2022). Focusing on
 108 carbonate base cations may avoid typical issues with C heterogeneity and detection of relatively small SIC changes.

109 Thirdly, Tessier et al. (1979) operationally defined a reducible soil pool where base cations are associated with iron
 110 (Fe) and manganese (Mn) (hydr)oxides. Dzombak & Morel (1990) modelled adsorption of Mg to hydrous ferric
 111 oxides (FeO(OH)), in which a surface hydroxyl group loses a proton and is replaced by a magnesium ion (FeOOH
 112 + Mg²⁺ ⇌ FeOMg⁺ + H⁺) and thereby decreases solute TA, and an Fourth, the oxidizable pool where cations are
 113 bound to SOM or sulfides.

114 ~~Dzombak & Morel (1990) modelled adsorption of Mg to hydrous ferric oxides (FeO(OH)), in which a surface~~
 115 ~~hydroxyl group loses a proton and is replaced by a magnesium ion (FeOOH + Mg²⁺ ⇌ FeOMg⁺ + H⁺) and thereby~~
 116 ~~decreases solute TA. ... In the fourth soil pool considered here, the oxidizable pool, SOM can form strong bounds~~
 117 with cations after deprotonation. In the fourth considered soil pool, the oxidizable pool, organic functional groups

118 ~~such as carboxylic and phenolic groups can form strong bounds with cations after deprotonation~~ (Kalinichev et al.,
119 2011; Tipping & Hurley, 1992). SOM can thus scavenge cations in both the exchangeable and oxidizable pool. The
120 binding strength between SOM and a cation determines whether the cation resides in the exchangeable or
121 oxidizable pool (as graphically schematized in (Blume et al., (2016), Fig. 5.6). Cations in the oxidizable pool are
122 expected to chemically stabilize organic matter due to strong cation bridging and inhibition of decomposing enzymes
123 (Rowley et al., 2018).

124 In conclusion, base cations in these soil pools could decrease solute TA after proton release and hence degas DIC
125 while potentially stabilizing SOM. Last, besides soil pools, also plants can scavenge base cations from solution.
126 Base cations that go to the plant pool can be recycled to the aqueous phase, either through decomposition of plants
127 in the field or through the food chain and sewage system, further complicating base cation mass balancing.

128 The undesirable side-effect of base cation scavenging (by plant/soil pools) is the release of protons to maintain
129 charge balance. This release of protons converts negatively charged DIC (HCO_3^- and carbonate anions (CO_3^{2-})) to
130 H_2CO_3 , which is in equilibrium with gaseous CO_2 ($\text{CO}_3^{2-} + \text{H}^+ \rightarrow \text{HCO}_3^-$ and $\text{HCO}_3^- + \text{H}^+ \rightarrow \text{H}_2\text{CO}_3 \Leftrightarrow \text{H}_2\text{O} + \text{CO}_2$
131 (g)). Hence, inorganic CO_2 removal can be reversed during temporary storage of base cations and realized again
132 when base cations are released back from soil and plant pools into the aqueous phase.

133 From base cations in plant and soil pools, we can thus calculate a 'potential inorganic CO_2 removal', a terminology
134 proposed by Steinwider et al., (2025). This is a maximum quantity of Inorganic CO_2 removal that can be achieved
135 when all cations released through silicate weathering are charge-balanced by bicarbonate/carbonates and leached
136 from soils. Base cation retention in different soil pools results in a temporal decoupling between weathering and
137 inorganic CO_2 removal. The timeframe in which the potential inorganic CO_2 removal can be achieved is a major
138 uncertainty in EW (Kanzaki et al., 2025). For weakly bound exchangeable cations, potential inorganic CO_2 removal
139 may be achieved in the relative short term of decades. Within this timeframe, because of stronger binding strengths,
140 reducible and oxidizable base cations are more unlikely to be released and thus deliver inorganic CO_2 removal.
141 Last, inorganic CO_2 removal is only achieved if the weathering agent that induced the weathering was H_2CO_3 (as
142 in Reaction 1-3). If the weathering agent is another acid (e.g. nitric acid (HNO_3) from fertilizers), no inorganic CO_2
143 removal occurs within the soil (McDermott et al., 2024; Taylor et al., 2021).

144 In a mesocosm experiment with basalt rock powder addition, we aimed to accurately quantify the W_r and potential
145 inorganic CO_2 removal through quantification of base cations in the four abovementioned soil pools, soil water and
146 maize plants. Tracing the fate of alkalinity after its generation by the weathering of primary minerals is key to
147 accurately quantify basalt W_r s. Here, we make a mass balance after 101 days of experiment, investigate the fate
148 of base cations through exploration of sequential extractions as a monitoring strategy for weathering and
149 implications for C sequestration.

2. Materials and Methods

2.1 experimental set-up

A mesocosm experiment with 30 mesocosms was constructed at the experimental site at the Drie Eiken Campus of the University of Antwerp (Belgium). This experiment was part of a larger mesocosm experiment that aimed to investigate heavy metal fate and plant biomass in silicate amended maize plants (Rijnders et al., 2025). The mesocosms (0.6 m height, radius=0.25m) received natural rainfall and received additional water through manual irrigation (**Fig. S2**). In May 2021, the lower 40 cm of each mesocosm was filled with a slightly acidic sandy loam soil (**Table 1**).

Table 1: Properties of control soil. w%=weight percent. *

Control soil properties*		Number of Replicates	Measuring method
pH (in a soil: water suspension (1:2.5))	5.66 ± 0.01	3x (before addition soil to pots)	(in a soil: water suspension (1:2.5))
Texture (Sand, clay, silt w%)	Sandy loam (61, 4, 35 w%)	3x (before addition soil to pots)	**
Soil organic C (SOC) (w%)**	0.53 ± 0.01	4x (0-20 cm)	***
SIC (w%)	0.0031 ± 0.0002	4x (0-20 cm)	carbonate extraction (see Equation S4 in supplement)
Cation exchange capacity (CEC) (meq/100g)	3.03 ± 0.11	15x (3 depths x 5 control pots)	(Brown, 1943)
Base saturation (%)	50 ± 5	15x (3 depths x 5 control pots)	(Brown, 1943)
Bulk density (BD) (kg/L)	1.58±0.02	14x (5x 0-20, 5x 20-30cm 4x 30-50cm)	Sampling soil cores (100 cm ³ , 5 cm length x 20 cm ²). And weigh after drying soil at 70°C for 48 hours
Fe-(hydr)oxide (mg Fe/g soil) ^{iv}	1.13±0.04	12x (4x 0-20, 4x 20-30cm 4x 30-50cm)	^{iv}

*Reported values represent the average ± standard error (SE) of control soil sampled at all depths after the experimental period of 101 days unless stated otherwise. ** Determined through loss on ignition (4h heating at 360°C and assuming a SOC/SOM ratio of 0.58). ** 40g of air dried soil was shaken for 18 hours with 100 mL of 50 g L⁻¹ sodium hexametaphosphate solution, sieved over 63 µm to separate sand from silt+clay. The same was done for a blank. The sieved solutions (sample and blank) were diluted with deionized water to one liter and after six hours density and temperature were measured. Clay = (density (sample) – density (blank)) / sample mass and silt= 100%-sand%-clay%. ***Determined through loss on ignition (4h heating at 360°C and assuming a SOC/SOM ratio of 0.58 (Van Bemmelen, 1890)). ^{iv} Estimation of the Fe (hydr)oxide content for control soil based on Fe in the reducible pool (method of extraction: see Table 3).

The upper 20 cm was filled with the same soil, either unamended in the control treatment (five mesocosms), or amended with basalt (**Figure 2**). Five mesocosms received 50 ton basalt ha⁻¹, while six others received different amounts of basalt, ranging between 10 and 200 ton ha⁻¹ (**Table 2**). The basalt was mixed homogenously in the control soil using a concrete mixer. Basalt was obtained from DURABAS (<https://www.rpbl.de>). Particle size distribution (PSD) was analyzed using a mastersizer 2000 with a Hydro 2000G sample dispersion unit after removing larger particles with a 2 mm sieve. The P80 was 310.78 µm (see **Fig. S5**). The specific surface area

173 (SSA) was determined with a Quantachrome Autosorb iQ using the Braunauer-Emmet-Teller (BET) method. The
 174 measurement used nitrogen gas as adsorbate with multi-point (5 points) and isotherm (77K) settings. Samples with
 175 the same treatment were pooled in equal quantities into one sample to reduce the cost and time for analysis. All
 176 samples were degassed at 300 °C with 200 minutes of soak time. High measurement quality was ensured by
 177 frequent reference measurements (Bundesanstalt für Materialforschung und -prüfung, Germany) in addition to three
 178 technical repetitions for each measurement. The BET-SSA of the basalt rock was $9.226 \pm 0.08 \text{ m}^2 \text{ g}^{-1}$. X-ray
 179 diffraction (XRD) and x-ray fluorescence (XRF) analyses are provided in the supplement.

180 **Table 2:** Overview of basalt application rates. The 0 and 50 t basalt ha⁻¹ application rates were replicated in five
 181 mesocosms, while other application rates were only tested in one mesocosm. We added these replicates within
 182 individual application rates to learn about the variability between mesocosms receiving the same treatment.

Ton silicate ha ⁻¹ (replications)	0 (5x)	10	30	50 (5x)	75	100	150	200
---	-----------	----	----	------------	----	-----	-----	-----

183
 184 Basalt was mixed into the top soil on 17/5/2021. To allow leachate collection, mesocosms had a 2 cm diameter
 185 hole at the bottom. On the inside, the bottom of the pot was covered with a root exclusion mesh to prevent soil
 186 export. Glass collectors (2.3L volume) were placed under the mesocosm to collect the leachates. Leachate volumes
 187 were determined throughout the experiment and were collected for chemical analyses on seven occasions. On
 188 3/6/2021, two sweet maize seedlings (variety Tom Thumb) were planted in each the mesocosms and all pots
 189 received fertilization with nitrogen (N), phosphorus (P) and potassium (K) (96 – 10 – 79) kg ha⁻¹ by adding Ca nitrate
 190 (Ca(NO₃)₂), triple super phosphate (TSP, 45% P₂O₅) and potassium sulfate (K₂SO₄). The experimental duration
 191 was 101 days; plants were harvested on 26/8/2021.

192 Soil water content and temperature were recorded using Cambell Scientific sensors (CS616) that are 30 cm in
 193 length. Watering (using rain water collected from a tank) was executed manually and total water manual inputs
 194 were tracked. In addition, daily precipitation amounts (in mm) were obtained for Wilrijk (Belgium) using the open
 195 source tool (visualcrossing.com). In the supplement, an overview of environmental conditions (rainfall, total water
 196 inputs, temperature and soil moisture) is given.

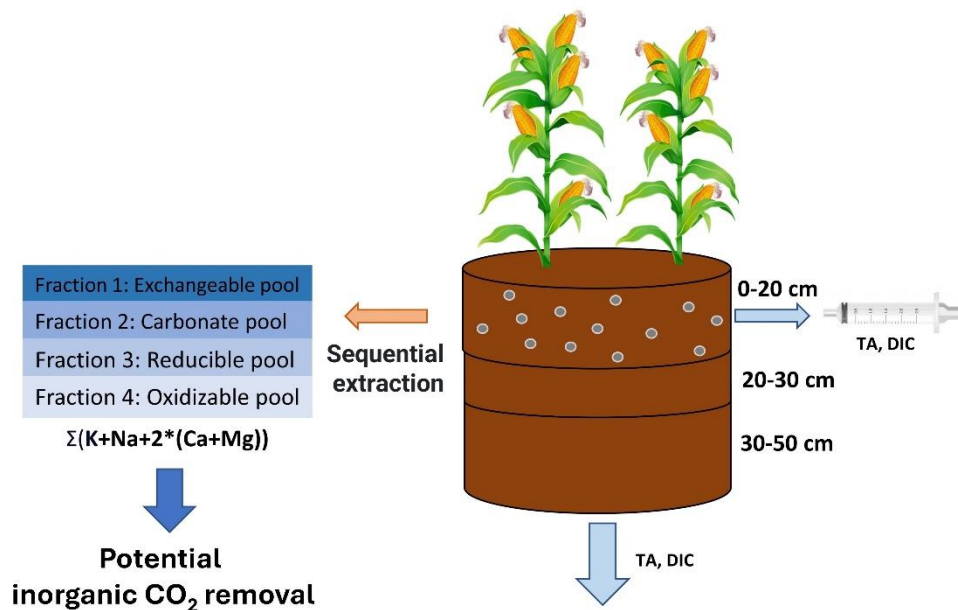


Figure 2: Overview of experimental set-up and measurements.

2.2 Leachate and pore water analysis

Weekly pore water sampling was performed with rhizons (Rhizon Flex, Rhizosphere Research Products B.V., Wageningen, NL) installed at 5 cm depth in each mesocosm. Leachate and porewater samples were filtered through a 0.45 μm PET filter. The major cations (Ca, Mg and K) were measured through ICP-OES (iCAP 6300 duo, Thermo Scientific). [Na was not directly measured in soil water samples; however, its charge contribution is accounted for indirectly in the measured soil water alkalinity.](#) Before analysis, ICP samples were conserved using 1.5 mL (HNO_3 69%) per 30 mL sample. TA was determined using a SAN++ continuous flow analyzer (Skalar - NLD). The pH was measured using a HI3220 pH/ORP meter. Dissolved organic carbon (DOC) and DIC were measured using a FormacsHT with LAS sampler (Skalar - NLD). DIC and DOC were measured on eight and 12 occasions in leachates and pore water respectively.

Two quality control (QC) standards were analyzed for individual elements (Ca, K, Mg, sodium (Na), [silicium-silicon](#) (Si) and Fe). The mean precision of the QC standards was 0.84%, 1.12%, 0.54%, 2.79%, 1.67% and 1.30% for the respective elements. The mean accuracy for the two QC standards was 1.87%, 2.30%, 0.17%, 1.88%, 1.39% and 2.65% for Ca, K, Mg, Na, Si and Fe respectively. For TA soil water samples, mean accuracy and precision for two different QC standards were 1.51 and 1.72% respectively. The DIC measurements with FormacsHT had an accuracy and precision 1.09 and 0.23% respectively. Accuracy and precision were determined based on 12 measurements of a QC for TA (standards: 150 and 350 $\text{mg CaCO}_3 \text{ L}^{-1}$) and DIC (range between 10 and 100 mg L^{-1}) and based on eight measurements of two different QC concentrations for each individual element.

219 **2.3 Soil collection and pretreatment**

220 Top soil pH was measured on five dates. To determine top soil pH, 4 g of air dried topsoil sample was dissolved in
221 10 mL deionized water and shaken before pH measurement using a HI3220 pH/ORP meter (Hanna Instruments,
222 Temse, Belgium). After harvesting, soils were sampled using cylindrical soil cores (100 cm³, 5 cm length x 20 cm²).
223 Samples were taken across the depth of the mesocosm and three sampling depths were considered (0-20cm, 20-
224 30cm, 30-50cm). One sample was taken for each depth and mesocosm. The cores were dried at 70°C for 48 hours
225 to determine water content (gH₂O/g soil) and bulk density. An additional soil sample was taken at each depth, dried
226 at 70 °C for 48 hours and used for chemical analyses after sieving over a 2 mm sieve, removing the majority of the
227 root biomass. Estimated base cations in sieved-off roots were negligible relative to soil pools and thus excluded
228 from our main cation budget.

229 **2.4 Sequential base cation extractions**

230 As conceptualized by Tessier et al. (1979), base cations can reside in four different soil pools: the exchangeable
231 pool (~~where O atoms on hydroxyl or carboxyl groups of clays or SOM associate with cations~~ cations weakly bound
232 to SOM or clays), the carbonate pool (cations bound in pedogenic carbonates), the reducible pool (cations bound
233 to Al/Mn/Fe hydr(oxide)) and the oxidizable pool (cations strongly bound to SOM). SOM bound to cations, extracted
234 with weak salt solutions in the exchangeable pool typically has a low turnover time (Poeplau et al., 2018) and is
235 therefore thought to be more susceptible to microbial decomposition than oxidizable SOM.

236 We adapted the original Tessier scheme by replacing 1M magnesium chloride with 1M ammonium acetate
237 (NH₄(CH₃COO)) for extraction of the exchangeable pool, in order to be able to measure all base cations in the
238 exchangeable pool. Likewise, Na-acetate was replaced with a mixture of acetic acid and water to be able to measure
239 Na in the carbonate pool. We quantified SIC changes from the base cations in these acetic acid extracts (as in
240 (Larkin et al., 2022)) (see also Equation S4). Additionally, three other SIC measurement techniques were explored
241 to compare and the sensitivity of detecting SIC changes after amending with a range of basalt (see section S3.7).

242 **Table 3: Overview of sequential extraction method**
243 (extraction time, temperature, conditions, volume of extractants and chemical composition of extractants).

244

Extraction scheme	Extraction scheme Adapted Tessier et al. (1979)*
Pool 1: Exchangeable pool	10 mL 1M NH ₄ (CH ₃ COO) 1h, 20°C, shaker → centrifuge → sample
Pool 2: Carbonate pool	5 mL 1M acetic acid (2h, 20°C, shaker) + 4 mL H ₂ O + 1 mL 3M NH ₄ Acetate → sample
Pool 3: Reducible pool	20mL 0.04M hydroxylamine (NH ₂ OH.HCl) in 25% (v/v) acetic acid (pH 2) 6h, 96°C, heat bath
Pool 4: Oxidizable pool	3mL 0.02M HNO ₃ +5mL 30% peroxide (H ₂ O ₂) (to pH 2 with HNO ₃): 2h, 85°C, heat bath +3mL 30%H ₂ O ₂ (to pH 2 with HNO ₃) 3h, 85°C, heat bath +5mL 3.2M NH ₄ (CH ₃ COO) (in 20 vol%HNO ₃) +4 mL H ₂ O 0.5h, 20°C, shaker

Prior to extractions, approximately 1g of soil was air dried. We also conducted the extractions for the pure basalt that was initially added to the mesocosms to be able to correct for the cations that were initially already present as exchangeable, carbonate, reducible and oxidizable pool cations. After each extraction, samples were centrifuged for 2 minutes at 2000 rpm, supernatants were collected for analysis. The remaining soil pellet after centrifugation was washed with 10 mL of demineralized water before the following step. Relevant elements (K, Na, Mg, Ca, Al, Fe and Si) were measured in each pool using ICP-OES (iCAP 6300 duo, Thermo Scientific) for each pool. Si was only assessed in the reducible pool and in the oxidizable pool to investigate whether Si forms amorphous oxides or allophane-like compounds or binds with organic matter. Al carbonates were not quantified here as naturally these carbonates are not commonly formed (Takaya et al., 2019).

2.5 Plant responses

On 26/8/2021 (101 days after basalt amendment in soils), the aboveground biomass was harvested and dried for 48h at 70 °C to determine dry weight. [For the results on root biomass we refer to \(Rijnders et al. -\(2025\)\)](#). Plant material was ground with an ultra-centrifugal mill (Model ZM 200, Retsch GmbH, Haan, Germany). Base cations (Ca, Mg and K) were measured through ICP-OES (iCAP 6300 duo, Thermo Scientific) in aboveground biomass to calculate plant base cation stocks. [Na was not measured in aboveground biomass, because the amount of weathered base cations accumulated in plants is relatively small compared to that in soils, we do not expect this omission to substantially affect our results.](#) Base cations were measured separately in all aboveground biomass parts: stems, leaves, flowers and maize ears.

2.6 Calculation of W_r and potential inorganic CO₂ removal

We use the delta (Δ) symbol to denote the difference relative to unamended control soil. Accordingly, we quantify ΔTA (the change in total alkalinity in the basalt-amended soil relative to the control) based on the difference in base cation concentrations between amended and unamended soils. As basalt only contains cations and no conservative anions, we assume that ΔTA can be quantified from the change in base cation charges (**Equation 1**).

$$\Delta TA \approx 2 * (\Delta Ca + \Delta Mg) + \Delta Na + \Delta K - \Delta \text{conservative anions}$$

with Δ conservative anions = 0

(1)

278 [We thus use a base cation accounting approach as also proposed by Bijma et al. \(2026\) and explicitly assume no](#)
279 [changes in conservative anions after basalt amendment. Still, nitrogen cycling processes \(nitrification and](#)
280 [denitrification\) may be sensitive to soil chemistry and may therefore differ between treatments. Further research is](#)
281 [needed to verify whether conservative anions such as nitrates and phosphates are affected by rock amendment.](#)

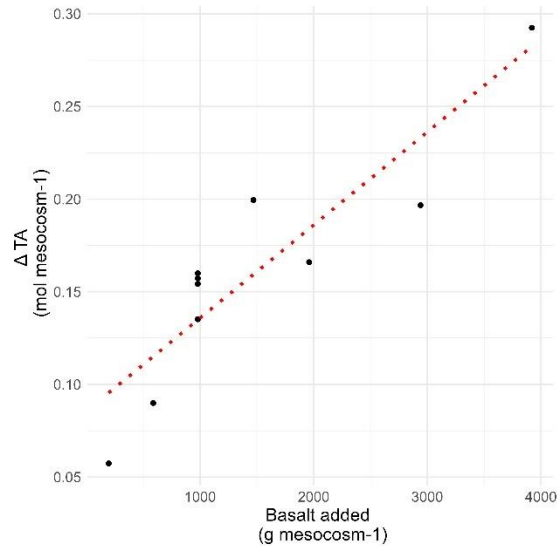
282 The W_r corresponds to the rate of rock dissolution. The W_r can be expressed per element or as moles of alkalinity
283 equivalents (i.e. the sum of base cation charges (**Equation 1**) per amount of rock surface area per unit of time (in
284 $\text{mol m}^{-2} \text{rock s}^{-1}$). In addition, we calculate a 'potential inorganic CO_2 removal'. We use the same definition for
285 potential inorganic CO_2 removal as in Steinwider et al. (2025). A 'potential inorganic CO_2 removal' can be defined
286 as the maximum amount of inorganic CO_2 that could be removed if all experimentally determined, weathered, soil-
287 retained base cations were to leach from the soil and be completely balanced by carbonate anions. Potential
288 inorganic CO_2 removal was previously 'CDR potential' by Niron et al. (2024)). The concept of CDR potential was
289 first introduced by Phil Renforth (2019) to describe the maximum inorganic CO_2 removal achievable if all base
290 cations within a rock were to completely weather. More recently, Beerling et al., (2024) quantified base cation losses
291 from topsoils using an immobile/mobile tracer approach (see Section 4.2), from which they also derived a measure
292 of CDR potential. To maintain conceptual clarity, we avoid using the term CDR potential for purposes other than its
293 original definition by Renforth (2019). When the term is employed, its meaning should always be explicitly stated.

294 To calculate the W_r (from all base cation increases relative to controls in plants, extracted soil fractions and soil
295 water leachates), we sum changes in TA in the following pools: exported soil water (leachates), plants and soil
296 pools. [Weathering rates are uncertain due to variability in soil cation pools considered, potential underestimation](#)
297 [from unextractable base cations in secondary minerals and methodological limitations in detecting all weathering](#)
298 [products.](#) We can express changes in the cation pool of each reservoir as the equivalent W_r required to supply the
299 cations ($W_{r\text{leachate}}$, $W_{r\text{plant}}$ and $W_{r\text{soil}}$) (**Equation 2**). Conventionally W_r s are expressed using a logarithmic scale as
300 absolute values can vary strongly.

$$301 \quad \text{Log } W_r \left[\frac{\Delta \text{mol TA}}{\text{m}^2 \text{rock.s}} \right] = \text{Log} \left(\frac{\Delta \text{mol TA}_{\text{soil}} + \Delta \text{mol TA}_{\text{plant}} + \Delta \text{mol TA}_{\text{leachate}}}{\text{m}^2 \text{rock.s}} \right) \quad (2)$$

302
303 We used a gradient of rock applications, where we calculated the slope of the molar change in base cation charges
304 (expressed as an equivalent "alkalinity" change if these base cations were dissolved in water) with higher rock
305 amendment (TA slope) (**Figure 3**). We compared logarithmic and linear regression and selected the linear
306 regression approach, as both approaches had comparable R^2 and Akaike Information Criterion (AIC) values values
307 and linear slopes ease further data processing (**Fig. S23 and Table S5**). We opted for the linear regression
308 approach to simplify subsequent calculations. To make our gradient approach more robust, we also calculated the
309 log W_r for individual application rates in **Fig. S13**.

310



311

312 **Figure 3:** Illustration of the calculation of TA slope: The alkalinity scavenging by a given pool was plotted in function
 313 of the applied basalt, after which the and the resulting slope was used to quantify the weathering ratea (Wr). This
 314 figure is an example regression with data for the top soil exchangeable pool. All regressions can be found in Fig.
 315 S22. Normalizing for mean control alkalinity equivalents before regression shifts the intercepts in Fig. S22 but does
 316 not affect the slope, preserving the relationship between basalt addition and the response variable (A. Gelman & J.
 317 Hill, 2007).

318 Then we converted units of the alkalinity slope for increasing rock application (TA slope) per unit of rock mass to
 319 moles of alkalinity per rock surface area and per time (Equation 3). Equation 3 was used to calculate $\Delta\text{mol TA m}^{-2}$
 320 rock s^{-1} of base cations in leachates, plants and of every measured soil pool at every soil depth.

$$321 \quad \frac{\Delta\text{mol TA}}{\text{m}^2 \text{ rock. s}} = \frac{\text{Scavenged alkalinity (= TA slope)} \left[\frac{\Delta\text{mol TA}}{\text{g rock}} \right]}{\text{Experimental duration [s]} * \text{SSA}_{\text{silicate}} \left[\frac{\text{m}^2 \text{ surface area}}{\text{g rock}} \right]} \quad (3)$$

322 $\Delta\text{mol TA m}^{-2} \text{ rock s}^{-1}$ was thus quantified per pool, based on the change in base cations in the basalt treatment
 323 compared to the control treatment. For plants, we calculate TA slope through regression of harvested base cations
 324 with basalt application. Harvested base cations were calculated as the product of harvested aboveground biomass
 325 and their base cation content. Charge contributions of Na were not included; Na was not quantified at the time of
 326 plant biomass elemental analysis, which may lead to an underestimation of the alkalinity equivalent increase in the
 327 plant pool. However, given that base cation charges in the plant pool were about two orders of magnitude smaller
 328 than in the soil pool, we expect the effect of this omission to be limited. In addition, maize plants aim to actively
 329 increase their K/Na ratio which avoids salt stress, the K content of maize shoots is typically about 2 orders of
 330 magnitude larger than Na (Gao et al., 2016; Suarez & Grieve, 1988). For leachates, TA slope was calculated as
 331 the product of mean cumulative leachate volume and mean leachate TA concentration for each application rate and
 332 regressing them with the applied basalt as dependent variable.

333 Finally, the Wr attributable to the change in cation content of the soil pools (Wr_{soil}) was calculated by summing the
 334 $Wr_{\text{soil_layer_k_pool_j}}$ for each pool and depth (Equation 4). Here, we sum changes in all pools of the topsoil (0-20 cm)
 335 and lower depths (20-30 cm and 30-50 cm) to obtain an aggregate value for Wr_{soil} . With

336 $Wr_{soil,layer k, fraction j}$ calculated as in **Equation 4** (with k = the number of depths and j = the number of considered
 337 soil pools). TA slope at every depth and soil pool was calculated as in **Equation 5**.

$$338 \quad Wr_{soil} = \sum_{k=1}^3 \sum_{j=1}^4 Wr_{soil,layer k, pool j} \quad (4)$$

$$339 \quad \frac{\text{scavenged TA (TA slope)} \left[\frac{\Delta \text{mol}}{\text{g rock}} \right]}{\frac{\frac{\mu \text{mol TA}}{\text{g dry Soil}} (\text{Amended Soil}) - \frac{\mu \text{mol TA}}{\text{g dry Soil}} (\text{control Soil})}{\text{Application rate (Amended soil)} [\text{g rock m}^{-2} \text{ ground area}] * 1000} * \text{Bulk Density} \left[\frac{\text{kg dry Soil}}{\text{m}^3 \text{ soil}} \right] * \text{thickness soil layer [m]}} = \quad (5)$$

340 Equivalents of soil retained base cation charge equivalents per gram of dry soil mixture can be calculated for each
 341 mesocosm by summing the charges from each base cation (**Equation 6**).

$$342 \quad \frac{\mu \text{mol TA}}{\text{g dry Soil}} = \sum_{j=1}^4 \left(\frac{\frac{\mu \text{g Ca}_{pool j}}{\text{g dry soil}}}{40.078 \frac{\text{gCa}}{\text{molCa}}} + \frac{\frac{\mu \text{g Mg}_{pool j}}{\text{g dry soil}}}{24.305 \frac{\text{gMg}}{\text{molMg}}} \right) * \frac{2 \text{mol TA}}{\text{mol cat}^{++}} + \left(\frac{\frac{\mu \text{g Na}_{pool j}}{\text{g dry soil}}}{22.990 \frac{\text{gNa}}{\text{molNa}}} + \frac{\frac{\mu \text{g K}_{pool j}}{\text{g dry soil}}}{39.098 \frac{\text{gK}}{\text{molK}}} \right) * \frac{1 \text{mol TA}}{\text{mol cat}^+} \quad (6)$$

343 These individual base cations (e.g. Ca in pool j) are calculated from the difference of cations weathered during the
 344 weathering operation minus the cations initially present in that fraction in the applied feedstock (Power et al., 2025)
 345 (**Equation 7**). For example, some cations can already exchange on the surface or edges of the applied minerals,
 346 so that these cannot be counted as weathered, they will however contribute to CDR once leached.

347 To calculate in-situ Wr , it is thus necessary to correct for the cations that had already been weathered from primary
 348 minerals at the time of silicate amendment. This correction is typically currently not being done in EW literature yet.
 349 As basalt is only added to the top soil and not deeper, this correction is only done for the 0-20 cm soil layer here.
 350 [A limitation of the approach in Equation 7 is that it assumes no physical transport of basalt to deeper soil layers,](#)
 351 [which may lead to underestimating weathered base cations in the 0–20 cm layer and overestimating them in the](#)
 352 [20–30 cm layer.](#)

$$353 \quad \frac{\mu \text{g element}_i \text{pool}_j}{\text{g dry soil}} = \left(\frac{\mu \text{g element}_i \text{pool}_j}{\text{g dry soil}} \right)_{\text{Post weathering, soil mixture}} - \left(\frac{\mu \text{g element}_i \text{pool}_j}{\text{g dry soil}} \right)_{\text{added with feedstock initially}} \quad (7)$$

354 The mass of a specific element (i) in each of the four (j) soil pools (in μg element/g soil) is calculated using **Equation**
 355 **8**.

$$356 \quad \left(\frac{\mu \text{g element}_i \text{pool}_j}{\text{g dry soil}} \right)_{\text{Post weathering, soil mixture}} = \frac{\text{concentration element}_i \text{ in pool}_j \left[\frac{\text{mg}}{\text{L}} \right] * \text{Volume extract}_j [\text{mL}]}{\text{mass of solid extracted [g]}} \quad (8)$$

357 The initial addition of element i to pool j is calculated as in **Equation 9**.

$$358 \quad \left(\frac{\mu \text{g element}_i \text{pool}_j}{\text{g dry soil}} \right)_{\text{added with feedstock initially}} = \frac{\mu \text{g element}_i \text{ pool}_j}{\text{g silicate}} * \frac{\text{Application rate} \left[\frac{\text{g silicate}}{\text{m}^2} \right]}{\text{Bulk density} \left[\text{g dry soil} \frac{\text{soil}}{\text{m}^3} \right] * \text{depth of soil amendment [m]}} \quad (9)$$

359 According to the charge balance (**Reaction 1-3**) during mineral dissolution, 1 mol HCO_3^- mol $^{-1}$ TA is generated (and
 360 thus 1 mol of CO_2 is sequestered). We define a factor η , that is equal to the ratio of HCO_3^- per mol of generated

361 TA. According to charge balance, $\eta=1$. A more conservative approach is to assume that all this generated alkalinity
 362 will be exported to the ocean, after which chemical equilibrium degasses a portion of the alkalinity ($\eta = 0.7 \text{ mol CO}_2$
 363 $\text{mol}^{-1} \text{ TA}$, assumed for oceans) (Renforth et al., 2012; Renforth et al., 2019; Renforth & Henderson, 2017).
 364 According to Renforth et al. (2019), the ocean alkalization efficiency η ranged between 0.7 and 0.85. This η
 365 parameter is relatively uncertain given that model studies indicate that η can range between 0.65 and 0.8 mol CO_2
 366 mol TA^{-1} (see section S6 in the supplement of (Kowalczyk et al., 2024)). Alternatively, we can assume that all base
 367 cations will form solid carbonates in soils or rivers. In this case $\eta=0.5 \text{ mol CO}_2 \text{ mol}^{-1} \text{ TA}$ (**Reaction 4**). In **Table 4**,
 368 we calculated potential inorganic CO_2 removals assuming conservative values of $\eta=0.5$ (carbonate precipitation
 369 scenario) and $\eta=1$ (the highest possible η without any downstream DIC losses).

370 While calculating W_r , cations added with the rock feedstock that were already weathered were subtracted as in
 371 **Equation 7**, yet these cations are not subtracted to calculate the potential inorganic CO_2 removal as base cations
 372 in weathered fractions of the rock feedstock can also leach to soil water whereby HCO_3^- is generated. Last, base
 373 cation changes in the plant pool were excluded from the potential inorganic CO_2 removal pool here, as a
 374 conservative approach we assume that base cations in plants will not reach the ocean. The latter assumption had
 375 a negligible impact on the potential inorganic CO_2 removal estimate (**Table 4**).

376

$$\begin{aligned}
 \text{potential inorganic CO}_2 \text{ removal} \left[\frac{\text{kg CO}_2}{\text{t rock}} \right] &= \text{Scavenged TA} \left[\frac{\text{mol TA}}{\text{g rock}} \right] * \frac{\eta \text{ mol CO}_2}{\text{mol TA}} * \frac{44 \text{g CO}_2}{\text{mol CO}_2} * 1000 \quad (10) \\
 \text{with} \left(\frac{\mu\text{g element}_{i_{\text{pool } j}}}{\text{g dry soil}} \right)_{\text{added with feedstock initially}} &= 0
 \end{aligned}$$

377

378

379

380 2.7 Calculation of the carbonate saturation indices (SIc) using Phreeqc

381 To assess whether carbonate precipitation was theoretically possible during this experiment, we calculated SIc for
 382 dolomite and calcite. For Mg and Ca the SIc as the logarithm of the ion activity product and the solubility product
 383 constant if dolomite and calcite ($\text{SIc} = \log \text{IAP/K}$). Minerals have the potential to precipitate when a $\log \text{SIc} > 0$ is
 384 reached although substantial oversaturation of calcite ($\log \text{SIc} > 1$) without calcite formation is possible in rivers due
 385 to ion inhibition, e.g. by phosphate (Morse et al., 2007; Zhang et al., 2022). Likewise, they are in equilibrium at a
 386 $\log \text{SIc} = 0$ and dissolve if $\log \text{SIc} < 0$. The R phreeqc package was used and the phreeqc.dat database was used.
 387 As an input, the experimental pore water (10 cm depth) composition of Mg and Ca was entered, as well as measured
 388 pH and TA. Daily SIc values were calculated by feeding unique combinations of Mg, Ca, pH and into the PHREEQC
 389 solution function for each day.

390

391 2.8 Data analysis

392 For SIc and elemental stocks in plant biomass, soil pools and soil water export, a linear regression with basalt
 393 application rate as a dependent variable was performed to test for a basalt effect. For measurements that were

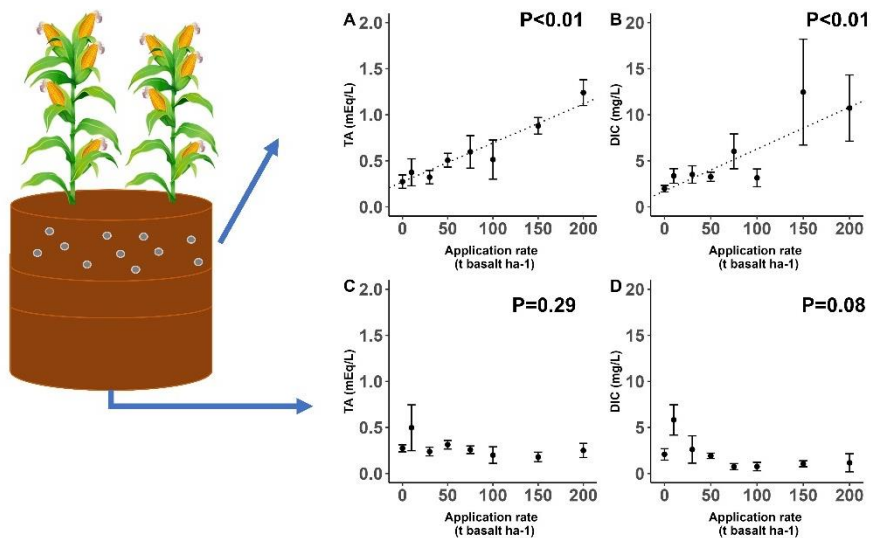
394 repeated in time (pore water and leachate DIC and DOC compositions), a linear mixed model was used with basalt
 395 and time as fixed factors and mesocosm as a random factor using the lme4 R package (version 1.1-33).
 396 For measurements repeated in time, we assessed basalt x time interaction effects and discarded these if not
 397 significant. All analyses were executed in R version 4.3.2. As an additional sensitivity analysis for the determination
 398 of W_r using the slope of application rates approach described in the main text, we quantified W_r also for individual
 399 application rates in **Fig. S13**.

400 To propagate uncertainty between basalt and controls in Figure 5, averages and standard errors for every replicated
 401 application rate (0 or 50 t/ha) were determined. The average from the 50 t ha⁻¹ was subtracted with the average
 402 from the control soil and $se = \sqrt{(se_control^2 + se_basalt^2)}$. For non-replicated application rates (10,30, 75,100,
 403 150 and 200 t/ha, $se=0$) the measurement was subtracted from the control soil average and errors were also
 404 propagated with $se = \sqrt{(se_control^2 + se_basalt^2)}$.

405 3 Results

406 Basalt amendment significantly increased DIC and TA in the top soil water (**Figure 4**). TA in soil water correlated
 407 positively with DIC ($R^2 = 0.68$, $p < 0.01$, **Fig. S10**). TA was thus generated in the basalt amended soil layer, yet we
 408 did not observe DIC or TA increases with higher basalt application rates in water exported from the soil column at
 409 60 cm depth (**Figure 4**). Temporal dynamics show that DIC in top soil pore water gradually increased in time with
 410 higher basalt amendment, while DOC decreased in time with more basalt (**Fig. S7 and Table S4**).

412



413 **Figure 4:** Top-soil (0-20 cm) pore water (A) TA and (B) DIC concentrations. Export water (50 cm depth) (C) TA and
 414 (D) DIC concentrations. Values represent average concentrations +- standard error across all sampling occasions
 415 over the 101-day experiment (n= 125, 44, 95 and 60 for pore water DIC, TA and leachate DIC and TA
 416 concentrations respectively). Significant trends are indicated with a dotted regression line. Raw data for TA and DIC
 417 in function of time is visualized in **Fig. S7(B,D)** and **Fig. S9(B,D)**.
 418
 419

420 Overall, base cations were mostly retained in the top soil, where Ca significantly increased in the exchangeable,
 421 reducible and oxidizable pools with higher basalt addition. Only in the carbonate soil pool, Ca (and also Mg)

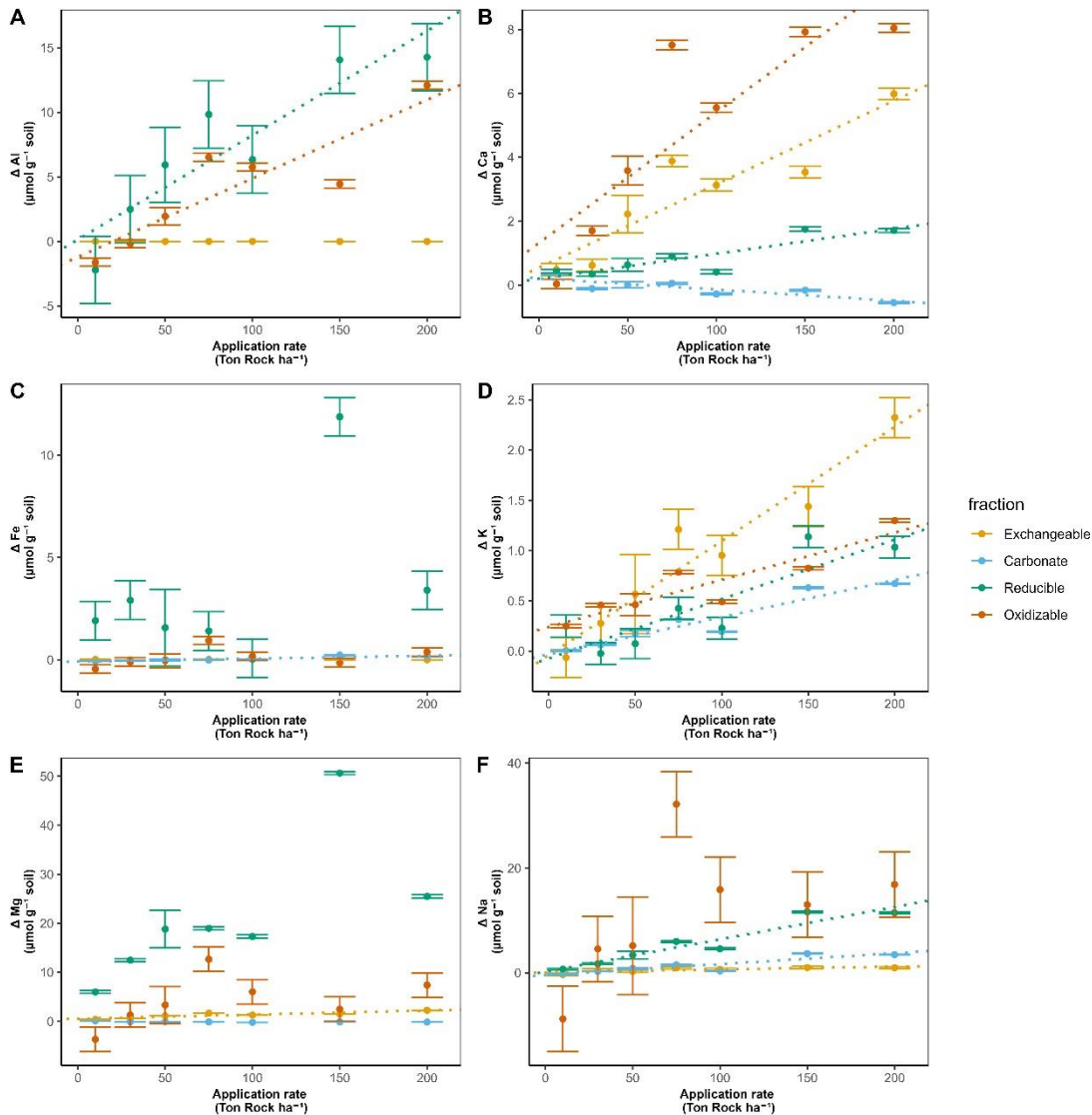
422 significantly decreased with more basalt (**Figure 5 and 6**). With higher rock amendment, Mg accumulated in the
423 top soil exchangeable pool ($p<0.01$). The Mg accumulation in the reducible pool was higher compared to the
424 exchangeable, but the slope was borderline significant for the reducible pool ($p=0.07$) due to higher variability in Mg
425 concentrations with increasing basalt amendment.

426 Changes in Na followed similar patterns as Mg, as also significantly more Na exchanged in top soil ($p=0.02$) and a
427 larger signal of reducible Na was found ($p<0.01$). In contrast with divalent cations, monovalent cations increased in
428 the carbonate fraction if basalt increased (**Figure 5 and 6**). With more basalt, Al is being found in association with
429 the oxidizable and reducible fraction. Si increased only significantly in the oxidizable pool ($p=0.04$) (**Fig. S15**).
430 Increases in oxidizable Si, Ca, Al with higher basalt addition suggest the formation of mineral-associated organic
431 matter.

432 In the soil layer just below the soil-basalt mixture (20-30 cm), the cations did not increase significantly in any of the
433 measured soil pools and oxidizable Na, Fe and Mg decreased significantly (**Fig. S11, Figure 6**). We did not observe
434 significant changes in any element with higher basalt amendment in the 30-50 cm soil layer (**Fig. S12**).

435

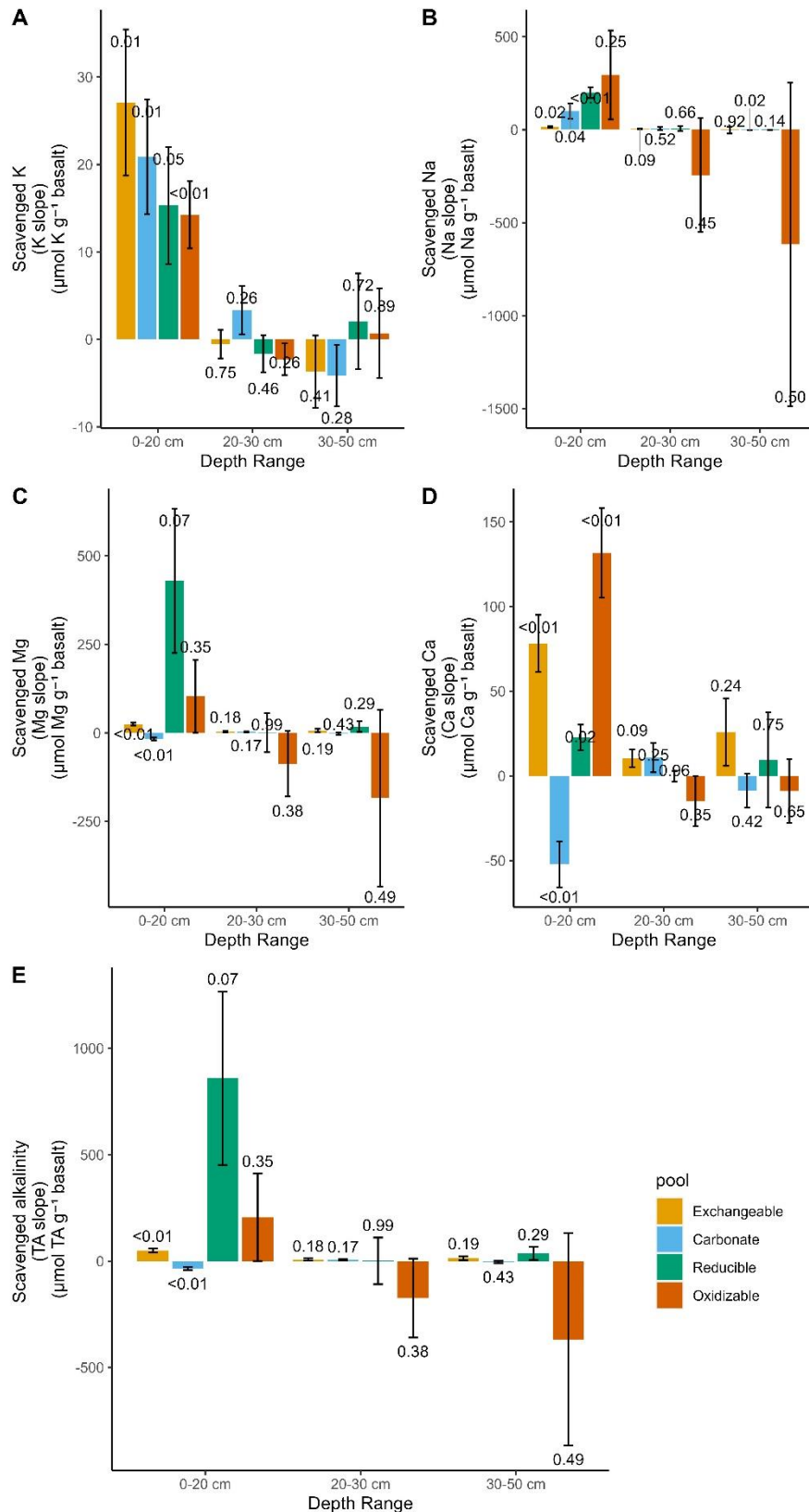
436



437
 438
 439 **Figure 5:** -Change in top-soil (0-20 cm) elements relative to the control soil (corrected as in Equation 7), 101 days
 440 after basalt amendment, as a function of basalt application rate for (A) Al (B) Ca (C) Fe (D) K (E) Mg and (F) Na for
 441 four different soil pools. Dots and error bars represent averages and standard errors. For basalt application rates
 442 other than 50 t ha⁻¹, error bars correspond to those of the control soils, as these basalt treatments were not
 443 replicated and the data are shown as control-normalized results. Significant effects (p < 0.05) of basalt application
 444 rate on cation concentrations are indicated by dotted linear regression lines. Measurements were repeated on at
 445 least four samples per fraction for the control soils (N ≥ 4 for each fraction) and N=4 for 50 t ha⁻¹ treatment (fewer
 446 than 5 replicates were available due to technical issues). Note that y-axes scales differ among subplots to better
 447 visualize small changes for some elements. Unnormalized (raw) data are presented in Fig. S19-21.

449 From all significant element changes in soil pools, we calculate that 8.4%, 52.1% and 9.4% Of basalt Na, K and Ca
 450 were weathered while we do not observe an increase in Mg if we only consider significant (p < 0.05) slopes. If we
 451 consider all (also p > 0.05) regression slopes, the estimates become 48.0%, 10.6%, 9.35% for K, Ca and Mg, while
 452 Na did not increase in this approach (mass balance per element, see Fig. S23).

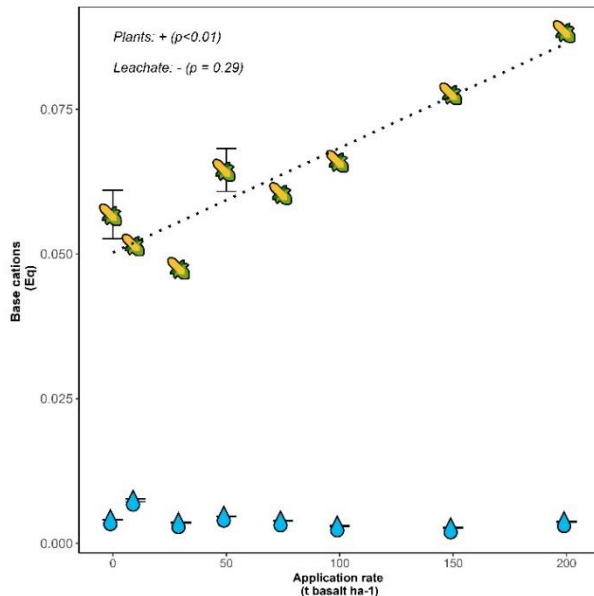
453



454
 455
 456
 457
 458
 459
 460
 461
 462

Figure 6: Equivalent alkalinity uptake 101 days after basalt amendment in different soil pools and depths. P-values of linear regressions are shown above and below bar plots of positive and negative changes respectively. Error bars represent the standard error that was derived from linear regression. Underlying regressions for slopes of TA scavenged by each pool and depth can be found in **Fig. S22**. Base cation changes in top-soil pore water are not included in this figure as we only include charge equivalent adsorbed by soil pools here, yet base cations in top soil pore water were negligible (see **Fig. S24**).

463 Base cations were not only scavenged by soils, but also by plants. Although two orders of magnitude smaller than
 464 in soil pools, TA scavenging by plants was higher than soil water exported TA and increased significantly with larger
 465 basalt amendment ($p < 0.01$) (**Figure 7**). The increase in base cation charges in plants was attributed to K (81%),
 466 Ca (11%) and Mg (8%).
 467



–**Figure 7: Moles of bBase cation charge equivalents**
 (Eq) per mesocosm after 101 days retained in maize
 plants (stems, leaves and maize ears), indicated with
 maize fruit symbols, and flushed with leaching water,
 indicated with droplets. Error bars represent averages
 and standard errors ($n=5$ for both control and 50 t ha^{-1}
 basalt replicates for plant measurements). For leachate
 TA, a total of 60 measurements were done in total at
 different dates. Na was not analyzed in plants and is
 thus not included in the harvested base cations. Errors
 on leachate TA were small and appear as horizontal
 lines within the droplets. Raw data for leachate TA
 measurements can be found in **Fig S9D**.

490
 491
 492
 493 Converting the base cations to moles of equivalent TA and considering only the exchangeable pool as only soil
 494 cation reservoir we derive a log weathering rate of $-12.13 \pm 0.34 \text{ mol TA m}^{-2} \text{ rock s}^{-1}$ (**Table 4**). When we consider
 495 also the decrease in base cation equivalents in the carbonate pool, the mean estimate decreases to -12.23 mol TA
 496 $\text{m}^{-2} \text{ rock s}^{-1}$, translating into mean estimated potential inorganic CO_2 removals of $0.36\text{-}0.715 \text{ kg CO}_2 \text{ t}^{-1} \text{ basalt}$
 497 (assuming $\eta=0.5$ -**10.7**). If we include all soil pools and non significant regressions the estimates becomes one order
 498 of magnitude higher, yet with substantial uncertainty.

499 **Table 4:** Overview of the Wr and potential inorganic CO_2 removal that can be quantified from changes in base
 500 cations in specific soil pools. Rows where (scavenged) TA increased significantly with increasing basalt amendment
 501 are indicated in bold.

Soil Pool	Depth	Reservoir	Log Wr (Log mol TA/m ² basalt /s)	CDR Potential* (kg CO ₂ /ton basalt) ($\eta = 0.5$)	CDR Potential* (kg CO ₂ /ton basalt) ($\eta = 1$)
/	/	Plant*	-12.93 ± 0.07	/	/
/	/	Leachate*	$Wr < 0$	/	/
Exchangeable	0-20cm	soil	-12.20 ± 0.41	1.10 ± 0.04	2.21 ± 0.07
Carbonate	0-20cm	soil	$Wr < 0$	-0.75 ± 0.03	-1.50 ± 0.06
Reducible	0-20cm	soil	-10.96 ± 0.21	18.91 ± 1.76	37.82 ± 3.51
Oxidizable	0-20cm	soil	-11.58 ± 0.43	4.53 ± 0.89	9.06 ± 1.77
Exchangeable	20-30cm	soil	-13.02 ± 0.29	0.17 ± 0.02	0.34 ± 0.04
Carbonate	20-30cm	soil	-13.17 ± 0.29	0.12 ± 0.02	0.23 ± 0.03
Reducible	20-30cm	soil	-	-	-
Oxidizable	20-30cm	soil	13.17 ± 50.43	0.02 ± 0.47	0.04 ± 0.95
Exchangeable	20-30cm	soil	$Wr < 0$	-3.82 ± 0.80	-7.56 ± 1.60
Exchangeable	30-50cm	soil	-12.76 ± 0.30	0.30 ± 0.04	0.61 ± 0.08
Carbonate	30-50cm	soil	$Wr < 0$	-0.10 ± 0.02	-0.21 ± 0.05
Reducible	30-50cm	soil	-12.34 ± 1.15	0.79 ± 0.13	1.58 ± 0.27

Oxidizable	30-50cm	soil	Wr<0	-8.10±2.15	-16.19±4.31
Exchangeable	0-20	Exchangeable+plant+leachate	-12.13±0.34	1.30±0.04	2.21±0.07
Exchangeable + Carbonate	0-20	Exchangeable+plant+leachate+ carbonate	-12.23±1.05	0.36±0.05	0.71±0.10
All soil pools	All	All soil pools + plant + leachate	-11.11±2.70**	13.17±3.07	26.33±6.13

502 *For leachates (which represents realized CDR) and also for plants there is no potential inorganic CO₂ removal in
503 this approach. ** Abs (Wr/standard error (Wr)*LN(10)) was used to propagate the error using the log10
504 transformation, resulting in substantial uncertainty for the Wr estimate of all pools.

505 4. Discussion

506 4.1 Weathering rates and CO₂ removal

507 EW is typically considered as a durable CDR pathway that removes CO₂ from the atmosphere by producing DIC
508 that is either transported to the ocean (Strefler et al., 2018) or precipitates as carbonates in the soil (Manning et al.,
509 2013). Here, we observe a clear weathering signal (a TA and DIC increase) in top soil pore water (**Figure 4**). These
510 TA and DIC increases in the pore water of amended top soil are consistent with recent findings (Holzer et al., 2023;
511 McDermott et al., 2024; Vienne et al., 2024). Increased DIC in basalt soils relative to controls may result from
512 enhanced plant ~~root respiration or~~ DIC exudation or from mineral weathering; our dataset does not allow these
513 effects to be separated. DIC did however not leach from our soil columns within this experimental timeframe of 101
514 days.
515

516
517
518 Absence of substantial DIC leaching is in line with other short-term recent studies (Amann et al., 2020; Larkin et al.,
519 2022; Niron et al., 2024; Vienne et al., 2024). For example, the log Wr of approximately -13 mol TA m² s⁻¹ quantified
520 from DIC export after 1 year in a mesocosm trial with 220 ton ha⁻¹ olivine-rich rock (Amann et al., 2020) was about
521 three orders of magnitude lower than what would be expected from lab-scale weathering studies (roughly -10 mol
522 TA m² s⁻¹, (Palandri & Kharaka, 2004)). Vienne et al. (2024), amended soils with 100 ton basalt ha⁻¹ and quantified
523 a CDR from exported TA that was in the same order of magnitude as in the work of Amann et al. (2020). Although
524 the studies of Amann et al. (2020), Vienne et al. (2024) were relatively short (<= 1 year) and used a relatively low
525 water infiltration flux, also a longer (3 year duration) catchment-scale study in Malaysian oil palm plantations with
526 high annual rainfall (>2000 mm year⁻¹) detected no significant increase in TA leaching in the catchments (Larkin et
527 al., 2022). There may thus be a substantial delay for DIC leaching.

528
529 A DIC leaching delay can have multiple causes (**Figure 1**); A first possibility is pedogenic carbonate formation.
530 We observe that solid carbonates did not increase in our experiment, in contrast, SIC decreased in time. PHREEQC
531 calculations for our experiment suggest that dolomite and calcite were undersaturated, so that carbonate dissolution
532 was possible (**Fig. S17**). Saturation states are expected to be low in our experiment because control soil was
533 undersaturated and dissolved base cations accumulated in other soil pools than the carbonate pool (**Figure 5 and**
534 **6**). A decrease in SIC is in contrast with substantial SIC increases found after wollastonite rock amendment (Haque

535 et al., 2019, 2020). The observed SIC increase in the latter field study may be partly attributed to residual carbonates
536 from prior liming activities instead of new carbonate formation related to silicate weathering (Haque et al., 2020).
537 Thus, not all measured SIC may reflect new carbonate formation in the study of Haque et al. (2020). For short-term
538 basalt studies, using elemental C analysis, also no significant changes in SIC could be detected previously (Kelland
539 et al., 2020; Vienne et al., 2022, 2024). In contrast, in the study of Larkin et al. (2022), a relatively small SIC increase
540 was detected in amended soils, using carbonate pool extractions.

541
542 While TA was not exported or taken up by soil carbonates here and plant base cation losses were minor (**Table 4**)
543 it was retained in top soil where the exchangeable and reducible pools reduced solute TA. We expect cations to be
544 primarily associated with Fe- and Mn-(oxyhydr)oxides in the reducible pool and with organic matter in the oxidizable
545 pool, as supported by literature (Tessier et al., 1979); However, the extraction chemicals of this sequential extraction
546 scheme (hydroxylamine and H₂O₂) are known to have a limited specificity and may have also partially targeted
547 other mineral phases (such as clays) (Ryan et al., 2008), which could explain the elevated Si observed in the topsoil
548 pools (**Fig. S15**). In addition, the observed increase of aluminum in association with the reducible soil fraction
549 indicate the formation of secondary minerals. While we cannot pinpoint the exact Mg-phases formed in our soils,
550 our results do demonstrate substantial base cation retention in the soil and show that there can be more base cation
551 losses to soils than to the exchangeable pool alone.

552
553 Our estimate of log W_r , derived solely from significant increases in TA uptake at higher basalt amendment rates,
554 was approximately $-12 \text{ mol TA m}^{-2} \text{ s}^{-1}$. This estimate reflects changes in the exchangeable and carbonate soil
555 pools, plant uptake, and leachate composition. Notably, this value aligns with previous studies that estimated log W_r
556 values between -12 and -11 based on base cation depletion from the exchangeable pool alone (Kelland et al.,
557 2020; Reershemius et al., 2023; te Pas et al., 2023), as summarized in Vienne et al., (2024). Also in a batch leaching
558 experiment with 1mM CaCl₂ (designed to mimic soil solutions) the quantified log W_r of basalt was found to be -11
559 (Van Der Bauwhede et al., 2024).

560
561 Estimates from Buckingham et al. (2022), based only on leachates, gave a much lower log W_r of -15 , partly due to
562 low water infiltration rates. With a high infiltration flux (8000 mm/year), Amann et al. (2022) estimated log W_r
563 between -12.5 and -13.5 from basalt leachates. This highlights the importance of including scavenged alkalinity to
564 determine W_r in soils. When we also include non-significant regression slopes we derive a mean log W_r estimate
565 with substantial uncertainty (-11.11 ± 2.70) mol TA $\text{m}^{-2} \text{ s}^{-1}$. From individual application rates, we quantify log W_r
566 ranging between -11 and -10 (**Fig. S13**); These values are comparable to those observed in soil-free, laboratory-
567 scale basalt dissolution experiments conducted at circumneutral pH (Brantley et al., 2008; Gislason & Oelkers,
568 2003). They also approximate the dissolution rates of key mineralogical components in basalt (such as plagioclases

569 (between -12 and -9 for Na and Ca endmembers respectively) and augite (-11.97)) under room temperature and
570 neutral pH conditions (Gudbrandsson et al., 2011; Hermanska et al., 2022; Palandri & Kharaka, 2004a).

571
572 Although this and other experiments show relatively consistent weathering rates from exchangeable base cations
573 (comparable to those observed in lab-scale studies) we emphasize that, unlike laboratory conditions where base
574 cations remain far from equilibrium in excess water, soils experience solid-phase cation scavenging, which
575 promotes DIC degassing (**Figure 1**). From the sum of significant TA slopes we calculate a relatively low potential
576 inorganic CO₂ removal, equalling to approximately 0.36-0.71 kg CO₂ ton⁻¹ basalt or 0.018-0.036 tCO₂ ha⁻¹ for a
577 basalt application rate of 50 t ha⁻¹ (**Table 4**). Also the highest possible potential inorganic CO₂ removal realized
578 within this experimental timeframe is modest; Including also non-significant TA increases and assuming $\eta = 1$, the
579 potential inorganic CO₂ removal is quantified to be 26.33±6.13 kg CO₂ ton⁻¹ basalt (**Table 4**). We emphasize that
580 a potential inorganic CO₂ removal is a maximum inorganic CO₂ removal that can be realized with the delivered
581 amount of base cation weathering as strong acids associated with fertilizers (such as nitric acid and sulphuric acid),
582 or organic acids and not carbonic acid may have initially weathered silicate rock which does not lead to a CDR
583 within the soil system (McDermott et al., 2024; Taylor et al., 2021). Moreover, life-cycle emissions associated with
584 mining, grinding and transporting rock are typically of the same order of magnitude as our relatively low potential
585 inorganic CO₂ removal (Lefebvre et al., 2019).

586
587 Furthermore, for climate change mitigation, not only the amount of potential inorganic CO₂ removal is important,
588 but also the timescale at which this CDR is realized (Kanzaki et al., 2025). A mass balance of base cations indicates
589 that exported TA was negligible compared to base cation charges that were retained in the soil over the timeframe
590 of our experiment (101 days) (**Table 4**). As long as TA is retained in soil pools, inorganic CO₂ removal through DIC
591 export is delayed as equivalent amounts of protons have then been released into the soil water to maintain charge
592 balance (**Figure 1**). Realization of this delayed inorganic CO₂ removal depends on liberation of base cations from
593 these soil pools and their transport out of the soil, charge-balanced by HCO₃⁻. This export may take decades or
594 longer, depending on the circumstances (Kanzaki et al., 2025).

595
596 The realization of CDR may be further delayed through the formation of base cation bearing clay minerals. Clay
597 formation has previously been suggested for EW application based on changes in soil water Ge/Si ratios and Si
598 isotopes (Vienne et al., 2024) and also based on Li isotope measurements (Pogge von Strandmann et al., 2022).
599 These measurements indicated basalt induced clay formation, but it remains unclear what type of clays were formed
600 and hence what the effect on inorganic CO₂ removal may be. In the best case for the inorganic CO₂ removal time
601 lag, the formed clays are 1:1 phyllosilicates such as kaolinite that do not sequester base cations. In this case, DIC
602 leaching is only retarded by base cation exchange. Worst case for the inorganic CO₂ removal time lag, the formed

603 secondary minerals bear substantial amounts of base cations ~~such (e.g. as) chlorite, or chrysotile, smectites,~~
604 [montmorillonites](#)). These clays exhibit a log W_r between -12 and -12.5 at neutral pH (Palandri & Kharaka, 2004),
605 so that dissolution within decadal timescales is unlikely (Bullock et al., 2022).

606

607 Although unfavourable for inorganic CO₂ removal, if base cation bearing secondary clay minerals would form, they
608 can increase SOC (Georgiou et al., 2022; Heckman et al., 2022; Steinwider et al., 2025). Georgiou et al. (2022)
609 refer to base-cation bearing clays (e.g. smectitic or illitic clays) as ‘high-activity minerals’ due to their higher SOM
610 stabilization capacity compared to secondary minerals that do not contain base cations (i.e., ‘low-activity minerals’,
611 with a lower CEC such as kaolinite). Both high- and low-activity minerals can adsorb DOC and form mineral-
612 associated organic matter-C (MAOM-C), which is believed to have a relatively high permanence (decades-
613 centuries) in soils (Lavalley et al., 2020). Besides mineral surface however, plant inputs can also limit SOC accrual.
614 In the latter case, SOC stocks can only increase if belowground plant C inputs increase, which could follow from
615 increases in exchangeable bases or pH (Haque et al., 2019; Shamshuddin et al., 2011). Nonetheless, increases in
616 decomposition can also stimulate SOC losses if rock dust increases soil pH (Klemme et al., 2022).

617

618

619 **4.2 Implications for monitoring inorganic CO₂ removal**

620

621 Different base cation monitoring strategies are possible. A first option is to quantify TA in soil water (Clarkson et
622 al., 2024). A disadvantage is however that soil water samples have to be sampled across the soil depth.
623 Alternatively, TA could be only monitored in top soil, yet then uncertain TA leaching models must be used (Kanzaki
624 et al., 2025). To calibrate TA leaching models, soil measurements in depth profiles could be used.

625

626 A first soil measurement approach is a total cation accounting approach, which quantifies the loss of base cations
627 from top soils (te Pas et al., 2025). However, this approach only focuses on the top soil and fails to account for
628 physical cation transport from top soils due to erosion or vertical feedstock transport via infiltration or bioturbation.
629 Alternatively, in a mobile/immobile tracer element approach (often named ‘TiCat’ by the EW community), cation
630 losses from amended top soils are quantified along with immobile tracers, which can account for cation losses
631 through bioturbation or erosion (Reershemius et al., 2023). Nonetheless the disadvantage of TiCat is that it does
632 not track potential TA scavenging (e.g. by organic matter or clays) at larger depth. Our potential inorganic CO₂
633 removal estimate will thus differ from a potential inorganic CO₂ removal estimate quantified using a TiCat approach.

634

635 Alternatively, entire depth profiles could be analyzed to spatially calibrate TA leaching models. Analysis of the
636 exchangeable soil pool is already a well-established method in EW research (Beerling et al., 2024; Reershemius et
637 al., 2023; Reynaert et al., 2023; Vienne et al., 2024). Adding also the carbonate, reducible and oxidizable soil pools

638 to the analysis could make base cation mass balancing more complete. These protocols could calibrate predictive
639 TA leaching models spatially. In addition there is an opportunity to quantify SOC and MAOM-C changes in the same
640 samples, which have recently gained traction in EW research due to their role in stabilizing SOM (Buss et al., 2024;
641 Sokol et al., 2024; Xu et al., 2024). Integration of these measurements can provide more accurate estimates of the
642 climate impact of EW, but should take into account the difference in permanence of inorganic and organic carbon
643 stocks.

644 However, this monitoring approach involves complexities such as feedstock correction, leaching solution strength
645 and soil heterogeneity. Although correcting for pre-weathered elements was crucial in this study, it assumes perfect
646 mixing based on a silicate-to-soil ratio. This correction was particularly significant for carbonate and reducible soil
647 pools, where for some base cations, over half of the cation increase with basalt amendment originated from
648 feedstock addition and not from weathering (**Fig. S18**). An alternative approach could involve creating time series
649 from sequential extraction data and quantifying base cation changes based on the change in time between multiple
650 measurements taken after rock amendment.

652 As discussed in the previous section, another key challenge is that the fate of base cations may remain uncertain
653 if strongly bound crystalline organo-minerals (see Lopez-Sangil & Rovira, 2013) form that are unextractable by the
654 Tessier scheme. Such processes may have contributed to the observed decrease in oxidizable elements at larger
655 depth, although this could also be an artefact of the applied extraction procedure. Pogge von Strandmann et al.
656 (2022) proposed substituting the H₂O₂ leaching step of the Tessier scheme with a dilute HCl leach, which is thought
657 to extract clays as well. Alternatively, post-extraction analysis of residual solids using techniques such as XRD or
658 QEMSCAN may be necessary to rigorously assess changes in rock mineralogy (Mason et al., 2022). Although deep
659 soil core sampling and extensive mineralogical analysis are resource-intensive and not feasible for large-scale
660 application, this monitoring strategy could be valuable during the initial adoption of EW in targeted 'measure-all'
661 experiments, as reliable TA leaching models require extensive calibration.

663

664 **5. Conclusions**

665 This study presents a detailed examination of EW and its effectiveness as a climate mitigation technique, revealing
666 both its potentials and limitations. A novel aspect of this work is the in-depth investigation of entire soil profiles for
667 base cations in different soil fractions, paired with soil water TA monitoring. We highlight the value of sequential
668 extractions as a method for monitoring base cations throughout soil profiles for calibrating TA leaching models.

669 Our findings indicate that basalt-based enhanced weathering may not immediately lead to the inorganic CO₂
670 removal previously anticipated in projections and IPCC reports (Babiker et al., 2022; Minx et al., 2018). We observed
671 rock weathering without inorganic CO₂ removal; despite the absence of DIC leaching or carbonate precipitation,

672 exchangeable bases increased with higher basalt amendments, demonstrating that rock weathering occurred.
673 Additionally, we observed a borderline significant but substantial increase in base cations in the reducible topsoil
674 pool with greater basalt application, which may further suppress TA leaching.

675 As base cation exchange increased with higher basalt amendments, we infer that greater application rates can
676 further delay the release of DIC from soil minerals to surface waters. However, in practice, EW is typically applied
677 at application rates below 30 t ha⁻¹. These lower, more practical rates may also enhance effectiveness of inorganic
678 CO₂ removal by reducing lag times for DIC release. It remains unclear if clays were formed here and whether EW
679 can deliver CDR within the urgent decadal timeframe needed to mitigate climate change. Despite its limitations for
680 short-term inorganic CO₂ removal, the generated secondary minerals and increased CEC could enhance plant
681 productivity and SOC retention in soils, contributing to long-term soil health, fertility, and potentially carbon
682 sequestration beyond inorganic pathways.

683 Acknowledgements

684 We thank Anne Cools, Steven Joosen and Anke De Boeck for their assistance with ICP-OES for sequential
685 extraction samples and Anthony De Schutter to characterize basalt using XRD. We thank DURUBAS to provide
686 basalt and provide the XRF material data sheet. We thank Tom Cox [and Jasper Roussard](#) for fruitful discussions.
687 We acknowledge the use of Microsoft Copilot [and Ecosia AI](#) to improve the English of this manuscript. This research
688 was supported by the Research Foundation— Flanders (FWO) [1S06325N], 1174925N] and [G000821N] (Biotic
689 controls of the potential of enhanced silicate weathering for land-based climate change mitigation). We also
690 acknowledge support of the UPSURGE project, which has received funding from the European Union’s Horizon
691 2020 research and innovation program under grant agreement No 101003818.

692 Author contribution

693 AV: research conceptualization, data gathering, development methodology, data analysis and writing. PF:
694 conceptualized sequential extraction methodology, writing and discussion. JR: research conceptualization, data
695 gathering. TJS: writing and discussion. TR: writing and discussion. RP: data gathering, rock characterization and
696 writing. JH: writing and discussion. HN: development extraction methodology, writing and discussion. MPE:
697 elemental C measurements and proofreading. LS: writing, development methodology and discussion. LB: writing
698 and discussion. SV: supervising research, conceptualization, writing and discussion.

699 Data and code availability

700 Data and code used in this manuscript are freely available at: <https://zenodo.org/records/15129984>

701

702 References

- 703 A. Gelman, & J. Hill. (2007). *Data analysis using regression and multilevel/hierarchical models*. Cambridge
704 University Press. https://moodle2.units.it/pluginfile.php/756424/mod_resource/content/1/gelman_hill_2007.pdf
- 705 Amann, T., & Hartmann, J. (2022). Carbon Accounting for Enhanced Weathering. *Frontiers in Climate*, 4(May), 1–
706 9. <https://doi.org/10.3389/fclim.2022.849948>
- 707 Amann, T., Hartmann, J., Hellmann, R., Pedrosa, E. T., & Malik, A. (2022). Enhanced weathering potentials—the
708 role of in situ CO₂ and grain size distribution. *Frontiers in Climate*, 4.
709 <https://doi.org/10.3389/fclim.2022.929268>
- 710 Amann, T., Hartmann, J., Struyf, E., De Oliveira Garcia, W., Fischer, E. K., Janssens, I., Meire, P., & Schoelynck,
711 J. (2020). Enhanced Weathering and related element fluxes - A cropland mesocosm approach.
712 *Biogeosciences*, 17(1), 103–119. <https://doi.org/10.5194/bg-17-103-2020>

- 713 Babiker, M., G. Berndes, K. Blok, B. Cohen, A. Cowie, O. Geden, V. Ginzburg, A. Leip, P. Smith, M. Sugiyama, F.
714 Y., & [P.R. Shukla, J. Skea, R. Slade, A. Al Khourdajie, R. van Diemen, D. McCollum, M. Pathak, S. Some,
715 P. Vyas, R. Fradera, M. Belkacemi, A. Hasija, G. Lisboa, S. Luz, J. Malley, (eds.)]. (2022). *Cross-sectoral*
716 *perspectives*. In IPCC, 2022: *Climate Change 2022: Mitigation of Climate Change. Contribution of Working*
717 *Group III to the Sixth Assessment Report of the Intergovernmental Panel on Climate Change*.
718 <https://doi.org/10.1017/9781009157926.005>
- 719 Barker, S. (2013). Dissolution of Deep-Sea Carbonates. In *Encyclopedia of Quaternary Science* (2nd ed., Vol. 2,
720 Issue 2002). Elsevier B.V. <https://doi.org/10.1016/B978-0-444-53643-3.00289-2>
- 721 Beerling, D. J., Epihov, D. Z., Kantola, I. B., Masters, M. D., Reershemius, T., Planavsky, N. J., & Reinhard, C. T.
722 (2024). Enhanced weathering in the US Corn Belt delivers carbon removal with agronomic benefits. *PNAS*,
723 1–10. <https://doi.org/10.1073/pnas>.
- 724 Bijma, J., Hagens, M., Hammes, J. S., Planavsky, N., Strandmann, P. A. E. P. Von, & Meeresforschung, H. P.-.
725 (2026). *Reviews and syntheses : Carbon vs . cation based MRV of Enhanced Rock Weathering and the issue*
726 *of soil organic carbon*. 53–75.
- 727 Blume, H., Brümmer, G. W., Horn, R., & Kögel-knabner, I. (2016). *Scheffer/Schachtschabel soil science*. Springer.
728 <https://doi.org/10.1007/978-3-642-30942-7>
- 729 Brantley, S. L., White, A. F., & Kubicki, J. D. (2008). Kinetics of water-rock interaction. In *Kinetics of Water-Rock*
730 *Interaction* (Issue January). <https://doi.org/10.1007/978-0-387-73563-4>
- 731 Brown, I. C. (1943). A rapid method of determining exchangeable hydrogen and total exchangeable bases of soils.
732 In *Soil Science* (Vol. 56, Issue 5, pp. 353–357). <https://doi.org/10.1097/00010694-194311000-00004>
- 733 Buckingham, F. L., Henderson, G. M., Holdship, P., & Renforth, P. (2022). Applied Geochemistry Soil core study
734 indicates limited CO₂ removal by enhanced weathering in dry croplands in the UK. *Applied Geochemistry*,
735 147(October), 105482. <https://doi.org/10.1016/j.apgeochem.2022.105482>
- 736 Bullock, L. A., Yang, A., & Darton, R. C. (2022). Kinetics-informed global assessment of mine tailings for CO₂
737 removal. *Science of The Total Environment*, 808, 152111. <https://doi.org/10.1016/j.scitotenv.2021.152111>
- 738 Buss, W., Hasemer, H., Ferguson, S., & Borevitz, J. (2024). Stabilisation of soil organic matter with rock dust
739 partially counteracted by plants. *Global Change Biology*, 30(1), 1–14. <https://doi.org/10.1111/gcb.17052>
- 740 Clarkson, M. O., Larkin, C. S., Swoboda, P., Reershemius, T., Suhrhoff, T. J., Maesano, C. N., & Campbell, J. S.
741 (2024). A review of measurement for quantification of carbon dioxide removal by enhanced weathering in soil.
742 *Frontiers in Climate*, 6(June). <https://doi.org/10.3389/fclim.2024.1345224>
- 743 Dietzen, C., Harrison, R., & Michelsen-Correa, S. (2018). Effectiveness of enhanced mineral weathering as a carbon
744 sequestration tool and alternative to agricultural lime: An incubation experiment. *International Journal of*
745 *Greenhouse Gas Control*, 74(January), 251–258. <https://doi.org/10.1016/j.ijggc.2018.05.007>
- 746 Dzombak, D. A., & Morel, F. M. M. (1990). *Surface complexation modeling*. John Wiley & Sons (A Wiley-
747 Interscience Publication).
- 748 Fuss, S., Lamb, W. F., Callaghan, M. W., Hilaire, J., Creutzig, F., Amann, T., Beringer, T., De Oliveira Garcia, W.,
749 Hartmann, J., Khanna, T., Luderer, G., Nemet, G. F., Rogelj, J., Smith, P., Vicente, J. V., Wilcox, J., Del Mar
750 Zamora Dominguez, M., & Minx, J. C. (2018). Negative emissions - Part 2: Costs, potentials and side effects.
751 *Environmental Research Letters*, 13(6). <https://doi.org/10.1088/1748-9326/aab9f9>
- 752 Gao, Y., Lu, Y., Wu, M., Liang, E., Li, Y., Zhang, D., Yin, Z., Ren, X., Dai, Y., Deng, D., & Chen, J. (2016). Ability to
753 remove Na⁺ and retain K⁺ correlates with salt tolerance in two maize inbred lines seedlings. *Frontiers in Plant*
754 *Science*, 7(NOVEMBER2016), 1–15. <https://doi.org/10.3389/fpls.2016.01716>
- 755 Georgiou, K., Jackson, R. B., Vindušková, O., Abramoff, R. Z., Ahlström, A., Feng, W., Harden, J. W., Pellegrini, A.
756 F. A., Polley, H. W., Soong, J. L., Riley, W. J., & Torn, M. S. (2022). Global stocks and capacity of mineral-
757 associated soil organic carbon. *Nature Communications*, 13(1), 1–12. <https://doi.org/10.1038/s41467-022-31540-9>
- 759 Gislason, S. R., & Oelkers, E. H. (2003). Mechanism, rates, and consequences of basaltic glass dissolution: II. An
760 experimental study of the dissolution rates of basaltic glass as a function of pH and temperature. *Geochimica*
761 *et Cosmochimica Acta*, 67(20), 3817–3832. [https://doi.org/10.1016/S0016-7037\(00\)00176-5](https://doi.org/10.1016/S0016-7037(00)00176-5)
- 762 Gudbrandsson, S., Wolff-Boenisch, D., Gislason, S. R., & Oelkers, E. H. (2011). An experimental study of crystalline
763 basalt dissolution from 2pH11 and temperatures from 5 to 75°C. *Geochimica et Cosmochimica Acta*, 75(19),
764 5496–5509. <https://doi.org/10.1016/j.gca.2011.06.035>
- 765 Haque, F., Santos, R. M., & Chiang, Y. W. (2020). Optimizing Inorganic Carbon Sequestration and Crop Yield With

- 766 Wollastonite Soil Amendment in a Microplot Study. *Frontiers in Plant Science*, 11(July), 1–12.
767 <https://doi.org/10.3389/fpls.2020.01012>
- 768 Haque, F., Santos, R. M., Dutta, A., Thimmanagari, M., & Chiang, Y. W. (2019). Co-Benefits of Wollastonite
769 Weathering in Agriculture: CO₂ Sequestration and Promoted Plant Growth [Research-article]. *ACS Omega*,
770 4(1), 1425–1433. <https://doi.org/10.1021/acsomega.8b02477>
- 771 Heckman, K., Hicks Pries, C. E., Lawrence, C. R., Rasmussen, C., Crow, S. E., Hoyt, A. M., von Fromm, S. F., Shi,
772 Z., Stoner, S., McGrath, C., Beem-Miller, J., Berhe, A. A., Blankinship, J. C., Keiluweit, M., Marín-Spiotta, E.,
773 Monroe, J. G., Plante, A. F., Schimel, J., Sierra, C. A., ... Wagai, R. (2022). Beyond bulk: Density fractions
774 explain heterogeneity in global soil carbon abundance and persistence. *Global Change Biology*, 28(3), 1178–
775 1196. <https://doi.org/10.1111/gcb.16023>
- 776 Holzer, I. O., Nocco, M. A., & Houlton, B. Z. (2023). Direct evidence for atmospheric carbon dioxide removal via
777 enhanced weathering in cropland soil. *Environmental Research Communications*, 5(10).
778 <https://doi.org/10.1088/2515-7620/acfd89>
- 779 Janssens, I. A., Roobroeck, D., Sardans, J., Obersteiner, M., Peñuelas, J., Richter, A., Smith, P., Verbruggen, E.,
780 & Vicca, S. (2022). *Negative erosion and negative emissions : Combining multiple land-based carbon dioxide*
781 *removal techniques to rebuild fertile topsoils and enhance food production.*
- 782 Kalinichev, A. G., Iskrenova-Tchoukova, E., Ahn, W. Y., Clark, M. M., & Kirkpatrick, R. J. (2011). Effects of Ca²⁺
783 on supramolecular aggregation of natural organic matter in aqueous solutions: A comparison of molecular
784 modeling approaches. *Geoderma*, 169, 27–32. <https://doi.org/10.1016/j.geoderma.2010.09.002>
- 785 Kanzaki, Y., Planavsky, N. J., Zhang, S., Jordan, J., Suhrhoff, T. J., & Reinhard, C. T. (2025). Soil cation storage is
786 a key control on the carbon removal dynamics of enhanced weathering. *Environmental Research Letters*,
787 20(074055).
- 788 Katarzyna A. Kowalczyk, Thorben Amann, Jessica Strefler, M.-E., Vorrath, Jens Hartmann, Serena De Marco, Phil
789 Renforth, S., & Foteinis, E. K. (2024). Marine Carbon Dioxide Removal by alkalization should no longer be
790 overlooked. *Environmental Research Letters*, December 2016, 11–14.
- 791 Kelland, M. E., Wade, P. W., Lewis, A. L., Taylor, L. L., Sarkar, B., Andrews, M. G., Lomas, M. R., Cotton, T. E. A.,
792 Kemp, S. J., James, R. H., Pearce, C. R., Hartley, S. E., Hodson, M. E., Leake, J. R., Banwart, S. A., &
793 Beerling, D. J. (2020). Increased yield and CO₂ sequestration potential with the C4 cereal Sorghum bicolor
794 cultivated in basaltic rock dust-amended agricultural soil. *Global Change Biology*, 26(6), 3658–3676.
795 <https://doi.org/10.1111/gcb.15089>
- 796 Klemme, A., Rixen, T., Müller, M., Notholt, J., & Warneke, T. (2022). Destabilization of carbon in tropical peatlands
797 by enhanced weathering. *Communications Earth and Environment*, 3(1), 1–9.
798 <https://doi.org/10.1038/s43247-022-00544-0>
- 799 Larkin, C. S., Andrews, M. G., Pearce, C. R., Yeong, K. L., Beerling, D. J., Bellamy, J., Benedick, S., Freckleton, R.
800 P., Goring-harford, H., Sadekar, S., & James, R. H. (2022). Quantification of CO removal in a large-scale
801 enhanced weathering field trial on an oil palm plantation in Sabah , Malaysia. *Frontiers in Climate*.
802 <https://doi.org/10.3389/fclim.2022.959229>
- 803 Lavallee, J. M., Soong, J. L., & Cotrufo, M. F. (2020). Conceptualizing soil organic matter into particulate and
804 mineral-associated forms to address global change in the 21st century. *Global Change Biology*, 26(1), 261–
805 273. <https://doi.org/10.1111/gcb.14859>
- 806 Lefebvre, D., Goglio, P., Williams, A., Manning, D. A. C., Carlos, A., Azevedo, D., Bergmann, M., Meersmans, J.,
807 & Smith, P. (2019). Assessing the potential of soil carbonation and enhanced weathering through Life Cycle
808 Assessment : A case study for Sao Paulo State , Brazil. *Journal of Cleaner Production*, 233, 468–481.
809 <https://doi.org/10.1016/j.jclepro.2019.06.099>
- 810 Lopez-Sangil, L., & Rovira, P. (2013). Sequential chemical extractions of the mineral-associated soil organic matter:
811 An integrated approach for the fractionation of organo-mineral complexes. *Soil Biology and Biochemistry*, 62,
812 57–67. <https://doi.org/10.1016/j.soilbio.2013.03.004>
- 813 Manning, D. A. C., Renforth, P., Lopez-Capel, E., Robertson, S., & Ghazireh, N. (2013). Carbonate precipitation in
814 artificial soils produced from basaltic quarry fines and composts: An opportunity for passive carbon
815 sequestration. *International Journal of Greenhouse Gas Control*, 17, 309–317.
816 <https://doi.org/10.1016/j.ijggc.2013.05.012>
- 817 Mason, J., Lin, E., Grono, E., & Denham, T. (2022). QEMSCAN® analysis of clay-rich stratigraphy associated with
818 early agricultural contexts at Kuk Swamp, Papua New Guinea. *Journal of Archaeological Science: Reports*,
819 42(February), 103356. <https://doi.org/10.1016/j.jasrep.2022.103356>
- 820 Matylda Hermanska , Martin J. Voigt, Chiara Marieni, Julien Declercq, E. O. (2022). *A comprehensive and internally*

- 821 *consistent mineral dissolution rate database : Part I : Primary silicate minerals and glasses*. 597(July 2021).
822 <https://doi.org/10.1016/j.chemgeo.2022.120807>
- 823 McDermott, F., Bryson, M., Magee, R., & van Acken, D. (2024). Enhanced weathering for CO₂ removal using
824 carbonate-rich crushed returned concrete; a pilot study from SE Ireland. *Applied Geochemistry*, 169(June),
825 106056. <https://doi.org/10.1016/j.apgeochem.2024.106056>
- 826 Minx, J. C., Lamb, W. F., Callaghan, M. W., Fuss, S., Hilaire, J., Creutzig, F., Amann, T., Beringer, T., De Oliveira
827 Garcia, W., Hartmann, J., Khanna, T., Lenzi, D., Luderer, G., Nemet, G. F., Rogelj, J., Smith, P., Vicente
828 Vicente, J. L., Wilcox, J., & Del Mar Zamora Dominguez, M. (2018). Negative emissions - Part 1: Research
829 landscape and synthesis. *Environmental Research Letters*, 13(6). <https://doi.org/10.1088/1748-9326/aabf9b>
- 830 Morse, J. W., Arvidson, R. S., & Lüttge, A. (2007). Calcium carbonate formation and dissolution. *Chemical Reviews*,
831 107(2), 342–381. <https://doi.org/10.1021/cr050358j>
- 832 Navarre-Sitchler, A., & Brantley, S. (2007). Basalt weathering across scales. *Earth and Planetary Science Letters*,
833 261(1–2), 321–334. <https://doi.org/10.1016/j.epsl.2007.07.010>
- 834 Niron, H., Vienne, A., Frings, P., Poetra, R., & Vicca, S. (2024). Exploring the synergy of enhanced weathering and
835 *Bacillus subtilis*: A promising strategy for sustainable agriculture. *Global Change Biology*, 30(9), 1–18.
836 <https://doi.org/10.1111/gcb.17511>
- 837 Öquist, M. G., Wallin, M., Seibert, J., Bishop, K., & Laudon, H. (2009). Dissolved Inorganic Carbon Export Across
838 the Soil / Stream Interface and Its Fate in a Boreal Headwater Stream. *Environmental Science & Technology*,
839 43(19), 7364–7369.
- 840 Palandri, J. L., & Kharaka, Y. K. (2004). A compilation of rate parameters of water-mineral interaction kinetics for
841 application to geochemical modeling. *USGS Open File Report, 2004–1068*, 71. [http://www.dtic.mil/cgi-](http://www.dtic.mil/cgi-bin/GetTRDoc?Location=U2&doc=GetTRDoc.pdf&AD=ADA440035)
842 [bin/GetTRDoc?Location=U2&doc=GetTRDoc.pdf&AD=ADA440035](http://www.dtic.mil/cgi-bin/GetTRDoc?Location=U2&doc=GetTRDoc.pdf&AD=ADA440035)
- 843 Poeplau, C., Don, A., Six, J., Kaiser, M., Benbi, D., Chenu, C., Cotrufo, M. F., Derrien, D., Gioacchini, P., Grand,
844 S., Gregorich, E., Griepentrog, M., Gunina, A., Haddix, M., Kuzyakov, Y., Kühnel, A., Macdonald, L. M.,
845 Soong, J., Trigalet, S., ... Nieder, R. (2018). Isolating organic carbon fractions with varying turnover rates in
846 temperate agricultural soils – A comprehensive method comparison. *Soil Biology and Biochemistry*,
847 125(April), 10–26. <https://doi.org/10.1016/j.soilbio.2018.06.025>
- 848 Pogge von Strandmann, P. A. E., Liu, X., Liu, C. Y., Wilson, D. J., Hammond, S. J., Tarbuck, G., Aristilde, L.,
849 Krause, A. J., & Fraser, W. T. (2022). Lithium isotope behaviour during basalt weathering experiments
850 amended with organic acids. *Geochimica et Cosmochimica Acta*, 328, 37–57.
851 <https://doi.org/10.1016/j.gca.2022.04.032>
- 852 Power, I. M., Hatten, V. N. J., Guo, M., Rausis, K., & Klyn-hesselink, H. (2025). Are enhanced rock weathering rates
853 overestimated? A few geochemical and mineralogical pitfalls. *Frontiers in Climate*, 6(January), 1–9.
854 <https://doi.org/10.3389/fclim.2024.1510747>
- 855 Reershemius, T., Kelland, M. E., Jordan, J. S., Davis, I. R., D'Ascanio, R., Calderon-Asael, B., Asael, D., Suhrhoff,
856 T. J., Epihov, D. Z., Beerling, D. J., Reinhard, C. T., & Planavsky, N. J. (2023). Initial Validation of a Soil-
857 Based Mass-Balance Approach for Empirical Monitoring of Enhanced Rock Weathering Rates. *Environmental*
858 *Science and Technology*, 57(48), 19497–19507. <https://doi.org/10.1021/acs.est.3c03609>
- 859 Renforth, P. (2012). The potential of enhanced weathering in the UK. *International Journal of Greenhouse Gas*
860 *Control*, 10, 229–243. <https://doi.org/10.1016/j.ijggc.2012.06.011>
- 861 Renforth, Phil. (2019). The negative emission potential of alkaline materials. *Nature Communications*, 10(1).
862 <https://doi.org/10.1038/s41467-019-09475-5>
- 863 Renforth, Phil, & Henderson, G. (2017). Assessing ocean alkalinity for carbon sequestration. *Reviews of*
864 *Geophysics*, 55(3), 636–674. <https://doi.org/10.1002/2016RG000533>
- 865 Reynaert, S., Vienne, A., De Boeck, H. J., D'Hose, T., Janssens, I., Nijs, I., Portillo-Estrada, M., Verbruggen, E.,
866 Vicca, S., & Poblador, S. (2023). Basalt addition improves the performance of young grassland monocultures
867 under more persistent weather featuring longer dry and wet spells. *Agricultural and Forest Meteorology*,
868 340(July), 109610. <https://doi.org/10.1016/j.agrformet.2023.109610>
- 869 Rijnders, J., Vienne, A., & Vicca, S. (2025). Effects of basalt, concrete fines, and steel slag on maize growth and
870 toxic trace element accumulation in an enhanced weathering experiment. *Biogeosciences*, 22(12), 2803–
871 2829. <https://doi.org/10.5194/bg-22-2803-2025>
- 872 Robert A. Berner. (1991). A model for Atmospheric CO₂ over phanerozoic time. *American Journal of Science*, 291,
873 339–376.

- 874 Rowley, M. C., Grand, S., & Verrecchia, É. P. (2018). Calcium-mediated stabilisation of soil organic carbon.
875 *Biogeochemistry*, 137(1–2), 27–49. <https://doi.org/10.1007/s10533-017-0410-1>
- 876 Ryan, P. C., Hillier, S., & Wall, A. J. (2008). Stepwise effects of the BCR sequential chemical extraction procedure
877 on dissolution and metal release from common ferromagnesian clay minerals: A combined solution chemistry
878 and X-ray powder diffraction study. *Science of the Total Environment*, 407(1), 603–614.
879 <https://doi.org/10.1016/j.scitotenv.2008.09.019>
- 880 Schindlbacher, A., Beck, K., Holzheu, S., & Borken, W. (2019). Inorganic Carbon Leaching From a Warmed and
881 Irrigated Carbonate Forest Soil. *Frontiers in Forest and Global Change*, 2(August), 1–13.
882 <https://doi.org/10.3389/ffgc.2019.00040>
- 883 Shamshuddin, J., Anda, M., Fauziah, C. I., & Omar, S. S. R. (2011). Growth of cocoa planted on highly weathered
884 soil as affected by application of basalt and/or compost. *Communications in Soil Science and Plant Analysis*,
885 42(22), 2751–2766. <https://doi.org/10.1080/00103624.2011.622822>
- 886 Smith, P., Davis, S. J., Creutzig, F., Fuss, S., Minx, J., Gabrielle, B., Kato, E., Jackson, R. B., Cowie, A., Kriegler,
887 E., Van Vuuren, D. P., Rogelj, J., Ciais, P., Milne, J., Canadell, J. G., McCollum, D., Peters, G., Andrew, R.,
888 Krey, V., ... Yongsung, C. (2016). Biophysical and economic limits to negative CO₂ emissions. *Nature Climate
889 Change*, 6(1), 42–50. <https://doi.org/10.1038/nclimate2870>
- 890 Sokol, N. W., Sohng, J., Moreland, K., Slessarev, E., Goertzen, H., Schmidt, R., Samaddar, S., Holzer, I., Almaraz,
891 M., Geoghegan, E., Houlton, B., Montañez, I., Pett-Ridge, J., & Scow, K. (2024). Reduced accrual of mineral-
892 associated organic matter after two years of enhanced rock weathering in cropland soils, though no net losses
893 of soil organic carbon. *Biogeochemistry Letters*, 167(8), 989–1005. <https://doi.org/10.1007/s10533-024-01160-0>
- 895 Steinwider, L., Boito, L., Frings, P. J., Niron, H., Rijnders, J., de Schutter, A., Vienne, A., & Vicca, S. (2025).
896 Beyond Inorganic C: Soil Organic C as a Key Pathway for Carbon Sequestration in Enhanced Weathering.
897 *Global Change Biology*, 31(7). <https://doi.org/10.1111/gcb.70340>
- 898 Steinwider, L., Boito, L., Frings, P., Niron, H., Rijnders, J., De Schutter, A., Vienne, A., & Vicca, S. (2025). Beyond
899 inorganic carbon : Soil organic carbon as key pathway for carbon sequestration in Enhanced Weathering.
900 *Global Change Biology*.
- 901 Strefler, J., Amann, T., Bauer, N., Kriegler, E., & Hartmann, J. (2018). Potential and costs of carbon dioxide removal
902 by enhanced weathering of rocks. *Environmental Research Letters*, 13(3). <https://doi.org/10.1088/1748-9326/aaa9c4>
- 904 Suarez, D. L., & Grieve, C. M. (1988). Predicting cation ratios in corn from saline solution composition. *Journal of
905 Experimental Botany*, 39(5), 605–612. <https://doi.org/10.1093/jxb/39.5.605>
- 906 Swoboda, P., Döring, T. F., & Hamer, M. (2021). Remineralizing soils? The agricultural usage of silicate rock
907 powders: A review. *Science of the Total Environment*, 807(150976), 18.
908 <https://doi.org/10.1016/j.scitotenv.2021.150976>
- 909 Takaya, Y., Wu, M., & Kato, Y. (2019). Unique environmental conditions required for dawsonite formation:
910 Implications from dawsonite synthesis experiments under alkaline conditions. *ACS Earth and Space
911 Chemistry*, 3(2), 285–294. <https://doi.org/10.1021/acsearthspacechem.8b00121>
- 912 Taylor, L., Driscoll, C., Groffman, P., Rau, G., Blum, J., & Beerling, D. (2021). Increased carbon capture by a silicate-
913 treated forested watershed affected by acid deposition. *Biogeosciences Discussions*, 1–29.
914 <https://doi.org/10.5194/bg-2020-288>
- 915 te Pas, E. E. E. M., Chang, E., Marklein, A. R., Comans, R. N. J., & Hagens, M. (2025). Accounting for retarded
916 weathering products in comparing methods for quantifying carbon dioxide removal in a short-term enhanced
917 weathering study. *Frontiers in Climate*, 2029(February), 1–10. <https://doi.org/10.3389/fclim.2024.1524998>
- 918 te Pas, E. E. E. M., Hagens, M., & Comans, R. N. J. (2023). Assessment of the enhanced weathering potential of
919 different silicate minerals to improve soil quality and sequester CO₂. *Frontiers in Climate*, 4.
920 <https://doi.org/10.3389/fclim.2022.954064>
- 921 Tessier, A., Campbell, P. G. C., & Bisson, M. (1979). Sequential Extraction Procedure for the Speciation of
922 Particulate Trace Metals. *Analytical Chemistry*, 51(7), 844–851. <https://doi.org/10.1021/ac50043a017>
- 923 Tipping, E., & Hurley, M. A. (1992). A unifying model of cation binding by humic substances. *Geochimica et
924 Cosmochimica Acta*, 56(10), 3627–3641. [https://doi.org/10.1016/0016-7037\(92\)90158-F](https://doi.org/10.1016/0016-7037(92)90158-F)
- 925 Van Bemmelen, J. (1890). Über Die Bestimmung Des Wassers, Des Humus, Des Schwefels, Der in Den Colloïdalen
926 Silikaten Gebundenen Kieselsäure, Des Mangans U. S. W. Im Ackerboden. *Die Landwirthschaftlichen
927 Versuchs-Stationen*, 37, 279–290.

- 928 Van Der Bauwhede, R., Muys, B., Vancampenhout, K., & Smolders, E. (2024). Geoderma Accelerated weathering
929 of silicate rock dusts predicts the slow-release liming in soils depending on rock mineralogy , soil acidity , and
930 test methodology. *Geoderma*, 441(November 2023), 116734.
931 <https://doi.org/10.1016/j.geoderma.2023.116734>
- 932 Van Straaten, P. (2006). Farming with rocks and minerals: Challenges and opportunities. *Anais Da Academia
933 Brasileira de Ciencias*, 78(4), 731–747. <https://doi.org/10.1590/S0001-37652006000400009>
- 934 Vienne, A., Frings, P., Poblador, S., Steinwider, L., Rijnders, J., Schoelynck, J., Vinduskova, O., & Vicca, S. (2024).
935 Earthworms in an enhanced weathering mesocosm experiment : Effects on soil carbon sequestration , base
936 cation exchange and soil CO₂ efflux. *Soil Biology and Biochemistry*, 199(June), 109596.
937 <https://doi.org/10.1016/j.soilbio.2024.109596>
- 938 Vienne, A., Poblador, S., Portillo-estrada, M., Hartmann, J., Ijehon, S., Wade, P., & Vicca, S. (2022). Enhanced
939 Weathering Using Basalt Rock Powder : Carbon Sequestration , Co-benefits and Risks in a Mesocosm Study
940 With *Solanum tuberosum*. *Frontiers in Climate*, 4(May), 1–14. <https://doi.org/10.3389/fclim.2022.869456>
- 941 Wolf-Gladrow, D. A., Zeebe, R. E., Klaas, C., Körtzinger, A., & Dickson, A. G. (2007). Total alkalinity: The explicit
942 conservative expression and its application to biogeochemical processes. *Marine Chemistry*, 106(1-2 SPEC.
943 ISS.), 287–300. <https://doi.org/10.1016/j.marchem.2007.01.006>
- 944 Xu, T., Yuan, Z., Vicca, S., Goll, D. S., Li, G., Lin, L., Chen, H., Bi, B., Chen, Q., Li, C., Wang, X., Wang, C., Hao,
945 Z., Fang, Y., & Beerling, D. J. (2024). Enhanced silicate weathering accelerates forest carbon sequestration
946 by stimulating the soil mineral carbon pump. *Global Change Biology*, 30(8), 1–17.
947 <https://doi.org/10.1111/gcb.17464>
- 948 Zhang, S., Planavsky, N. J., Katchinoff, J., Raymond, P. A., Kanzaki, Y., Reershemius, T., & Reinhard, C. T. (2022).
949 River chemistry constraints on the carbon capture potential of surficial enhanced rock weathering. *Limnology
950 and Oceanography*, 67(S2), S148–S157. <https://doi.org/10.1002/lno.12244>

951